TECHNISCHE UNIVERSITÄT WIEN
Vienna University of Technology

MASTER THESIS

Real-time integration of bio-signals for personalized synchronized vagus nerve stimulation

by

BOGDAN George Raoul
11831515

Supervised by

Univ.-Ass. DI Babak Dabiri Razlighi

Univ. Prof. Dipl.-Ing. Dr. tech. Eugenijus Kaniusas

Vienna, February 2023

Abstract

The use of electrical stimulation of the vagus nerve as a treatment for neurological or mental disorders has gained significant attention in recent years. One of the newest and most convenient methods of stimulating the vagus nerve is through auricular vagus nerve stimulation. This method involves modulating the afferent vagus nerve and thus impact a wide range of physiological processes. In order to maximize the efficiency of the stimulation, it is crucial to monitor the physiological processes during stimulation and adjust the stimulation accordingly. Such monitorization can be achieved by using a closed-loop stimulation with biofeedback.

This thesis examines the effectiveness of using the MAX30001 sensor in a closed-loop biofeedback auricular vagus nerve stimulation device. The sensor is ideal for this application due to its ability to measure both electrocardiogram and bioimpedance data simultaneously, easy integration into wearable devices, and integrated signal filtering and communication via the SPI protocol. The sensor was utilized with MATLAB for data recording, analysis, and real-time visualization. A platform for adaptive auricular vagus nerve stimulation was previously developed in Simulink, which was modified and used to test and validate the use of the MAX30001 sensor in a closed-loop auricular vagus nerve stimulation.

The MAX30001 sensor was found to be compatible with the STM LQFP64 microcontroller for the purpose of closed-loop auricular vagus nerve stimulation. The microcontroller is capable of configuring data acquisition, timestamping the data, and saving the data to local memory or transmitting it to another device. Additionally, it is able to manage data processing and activation of the stimulator. Communication between the two devices was achieved through the use of the SPI protocol at speeds up to 12 MHz, allowing for data to be acquired, processed, and transmitted in approximately 24 ms.

The developed system was integrated with the aforementioned simulation platform. After calibration, a simulation of the closed loop auricular vagus nerve stimulation was done. In this simulation the microcontroller was able not only to acquire, process and send the data to the simulation, but also receive a command from the simulated stimulator.

Although there is still some work to be done to use this sensor at its full potential, the initial results are promising. Using the bioimpedance module from the sensor could drastically increase the accuracy of the stimulation and bring another layer of personalization. Also, integrating both the sensor and the stimulator in a single stand-alone device would make the closed loop personalized vagus nerve stimulator easier for patients to use.

Kurzfassung

Der Einsatz von elektrischer Stimulation des Nervus vagus zur Behandlung von neurologischen oder psychischen Störungen hat in jüngster Zeit eine beträchtliche Aufmerksamkeit auf sich gezogen. Eine der neuesten und bequemsten Methoden zur Stimulation des Nervus vagus ist die aurikuläre Vagusnervenstimulation. Diese Methode beinhaltet die Modulation des afferenten Nervus vagus und beeinflusst somit eine Vielzahl physiologischer Prozesse. Um die Effizienz der Stimulation zu maximieren, ist es wichtig, die physiologischen Prozesse während der Stimulation zu überwachen und die Stimulation entsprechend anzupassen. Eine solche Überwachung kann durch den Einsatz einer geschlossenen Schleife mit Biofeedback erreicht werden.

Diese Arbeit untersucht die Wirksamkeit des Einsatzes des MAX30001-Sensors in einem geschlossenen Schleifen-Biofeedback-aurikulären Vagusnervenstimulationsgerät. Der Sensor eignet sich ideal für diese Anwendung aufgrund seiner Fähigkeit, sowohl Elektrokardiogramm- als auch Bioimpedanzdaten gleichzeitig zu messen, einfach in tragbare Geräte integriert zu werden und integrierte Signalfilterung und Kommunikation über das SPI-Protokoll zu bieten. Der Sensor wurde mit MATLAB für Datenaufzeichnung, Analyse und Echtzeitvisualisierung verwendet. Eine Plattform für adaptive aurikuläre Vagusnervenstimulation wurde bereits in Simulink entwickelt, die modifiziert und verwendet wurde, um den Einsatz des MAX30001-Sensors in einer geschlossenen Schleife aurikulären Vagusnervenstimulation zu testen und zu validieren.

Der MAX30001 Sensor wurde für die Verwendung in einem geschlossenen Regelkreis-System für die aurikuläre Vagusnervenstimulation kompatibilisiert. Der STM LQFP64 Mikrocontroller konfiguriert Datenerfassung, timestampt die Daten und speichert sie im lokalen Speicher oder überträgt sie an ein anderes Gerät. Zudem verwaltet er Datenverarbeitung und Aktivierung des Stimulators. Kommunikation zwischen den Geräten erfolgte über das SPI-Protokoll mit Geschwindigkeiten bis zu 12 MHz, wodurch Daten in ca. 24 ms erfasst, verarbeitet und übertragen werden können.

Das entwickelte System wurde mit der oben genannten Simulationsplattform integriert. Nach der Kalibrierung wurde eine Simulation des geschlossenen Regelkreises für die aurikuläre Vagusnervenstimulation durchgeführt. Hierbei konnte der Mikrocontroller nicht nur Daten erfassen, verarbeiten und an die Simulation senden, sondern auch einen Befehl vom simulierten Stimulator empfangen.

Die ersten Ergebnisse sind vielversprechend, obwohl noch Arbeit zu leisten ist, um das volle Potenzial des Sensors zu nutzen. Die Verwendung des Bioimpedanzmoduls des Sensors könnte die Genauigkeit der Stimulation drastisch erhöhen und eine weitere Ebene der Personalisierung bringen. Darüber hinaus würde die Integration des Sensors und des Stimulators in einem einzigen Standalone-Gerät die Verwendung des personalisierten Vagusnerven-Stimulators für Patienten erleichtern.

Table of Contents

1 Introduction 6
1.1 Vagus Nerve 6
1.2 Clinical and potential uses of vagus nerve stimulation 9
1.3 Stimulation Methods 11
1.4 Personalization of Vagus nerve stimulation 14
2 Methods 16
2.1 Bio-Sensors 16
2.2 Microcontroller 21
2.4 MATLAB and Simulink 25
2.5 RealTerm Serial Monitor 26
2.6 BIOPAC system 26
2.7 Functional Validation of MAX30001 27
3 Results 33
3.1 Implementation with STM LQFP64 33
3.2 Integration with MATLAB 44
3.3 Adaptive stimulation platform integration 50
3.4 Comparing MAX30001 with BIOPAC 56
4 Discussion and Future work 59
5 References 61
6 Table of Figures 66
7 Table of tables 68

List of Abbreviations

VN	Vagus nerve
aVN	Auricular vagus nerve
VNS	Vagus nerve stimulation
aVNS	Auricular vagus nerve stimulation
ECG	Electrocardiograma
BioZ	Bioimpedance
AFE	Analog front end
NTS	Nucleus tractus solitarii
CNS	Central nervous system
SPI	Serial protocol interface
UART	Universal asynchronous receiver-transmitter
GPIO	General purpose input output
RTC	Real time clock
GUI	Graphical user interface
FIFO	First In First Out

1 INTRODUCTION

1.1 VAGUS NERVE

Sensory systems provide information to the brain about the exterior world and the interior environment within us. Classical research has revealed how external senses work, such as photoreceptors, sound, temperature, force, and chemicals through out the brain circuits which interpret sensory properties and elicit perceptions and motor responses. Parallel to this, the interoceptive nervous system sends sensory information from almost every organ system in the body to the brain, which ensures that key physiological needs are met.

A primary sensor channel is the Vagus nerve. It connects the body to the brain and is necessary not only for survival, but also for recovery purposes. Although vagal neurons make up a small percentage of the nervous system, they are responsible for a vast range of critical tasks.

The Vagus Nerve or the 10th Cranial Nerve is the longest and most extensively distributed of all cranial nerves. It was given this name because of its wandering path through the thorax and abdomen. The vagus nerve emerges laterally behind the olive from the medulla oblongata as a group of rootlets. After passing through the foramen jugulare, it forms a smaller, somatosensitive superior ganglion and a larger, viscerosensitive inferior ganglion. In the further course of the nerve, one can distinguish a head, a neck, a thoracic, and an abdominal part (Trepel, 2017). The auricular branch starts at the jugular ganglion, here the auricular vagus nerve has its bodies of the sensory ganglionic neurons, just outside the cranium (Nomura, 1984). Specific regions of the external ear are sensory innervated by the endings of the auricular vagus nerve. Some regions of the external ear are innervated by greater auricular nerve, auriculotemporal nerve and the auricular branch of the vagus nerve. At the same time, the middle region of the pinna, the central concha, is mostly innervated by auricular vagus nerve and the cymba concha region is 100% innervated only by the auricular vagus nerve (Peuker, 2002).

By convention, vagus nerve is referred to in the singular even though there is a left and a right one, each having some functional differences; for example, the sinoatrial node is innervated by the right vagus nerve, while the left one innervates the atrioventricular node (Thompson, 2020).

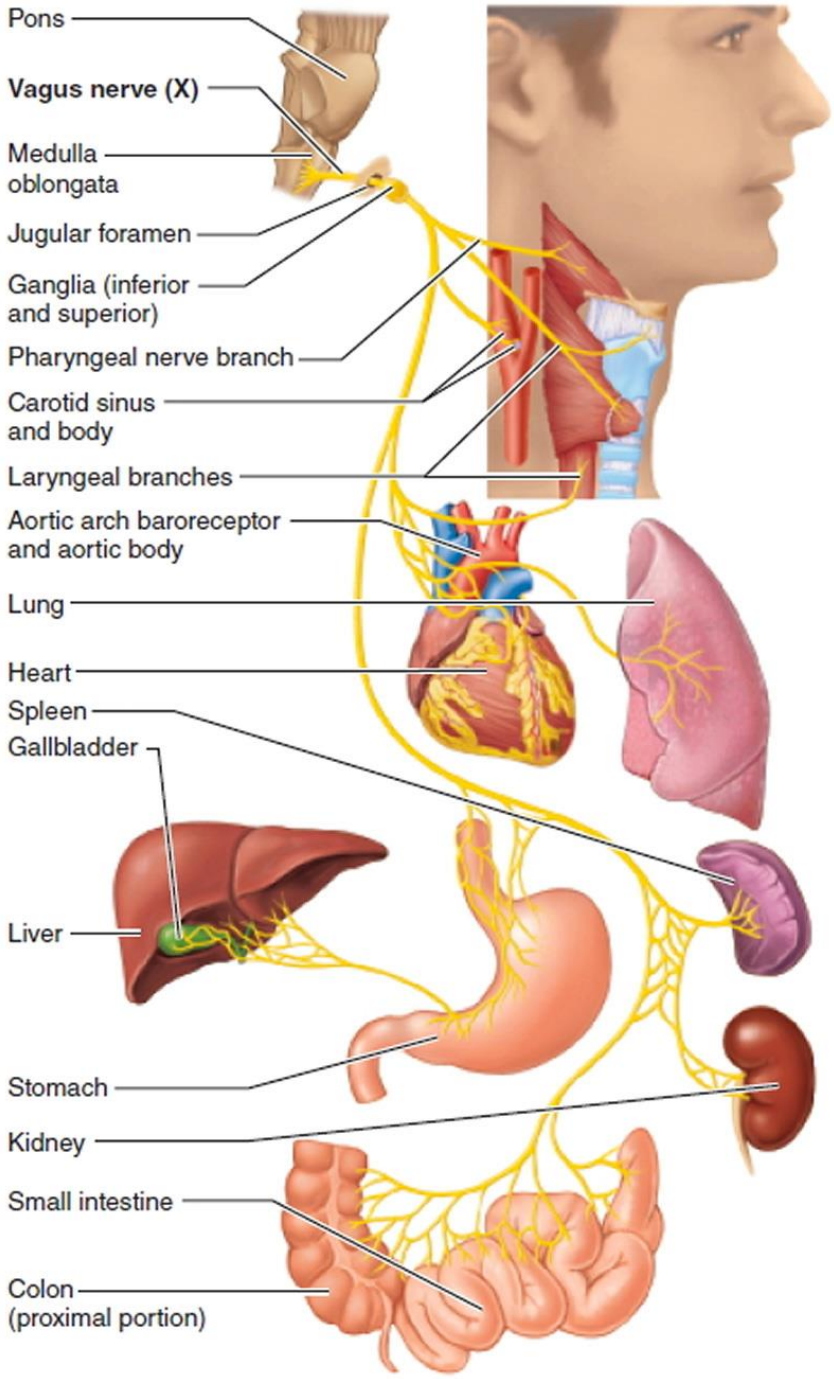

Figure 1.1.1 – Vagus nerve pathway (Polyvagal theory, 2022)

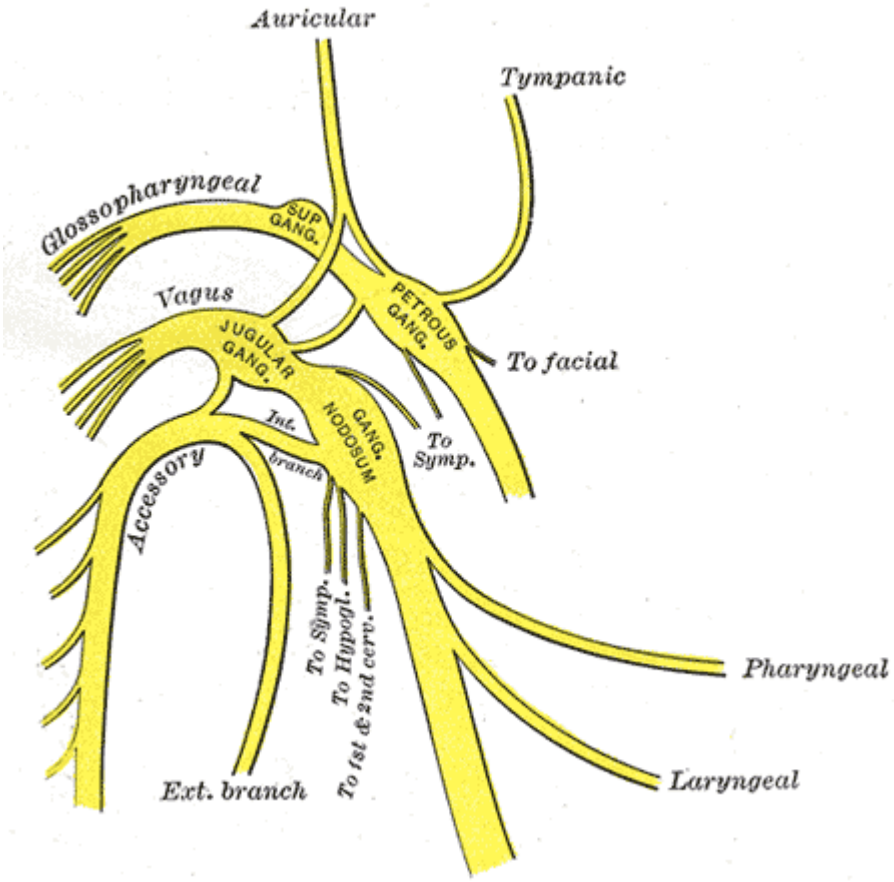

Figure 1.1.2 - Plan of upper portions of glossopharyngeal, vagus, and accessory nerves. (Gray, 1918)

According to Foley and DuBois, most neurons (~80%) within the vagus nerve are sensory neurons, bundled together with the motor neurons (Foley, 1937). The majority of the fibers provide the brain with the sensory information from mechanoreceptors, chemoreceptors, thermoreceptors, and osmoreceptors (Berthoud, 2000). Together with the efferent fibers, they respond according to the state of the body, through a closed-loop reflex. Example of responses are thermo-regulation, immune regulation, and blood pressure control (Kaniusas, 2019). Functionally, stimulating different locations in the ear, various physiological effects can occur. In rats for example, variable intensity of induced autonomic changes was shown as a function of the area of stimulation (Gao, 2007).

The vagus nerve has four categories of conduction, it has four different cranial nerve nuclei areas in the brainstem: Ncl. ambiguus (specific-visceromotor), Ncl. dorsalis n. vagi (general-visceromotor), Ncl. spinalis n. trigemini (general-somatosensory), and Nucleus tractus solitarii (NTS) (general- and specific-viscerosensory) (Trepel, 2017). The vagal afferent fibers influence the CNS through projections of these nuclei in the brain stem (Kaniusas, 2019). Due to these projections to the higher brain regions, allows the vagus nerve to modulate subcortical and cortical brain areas (Berthoud, 2000). This implies

that vagus nerve stimulation can influence basic brain functions, affecting the entire body in numerous ways. When stimulating the auricular vagus nerve, sensory fibers of the nerve are recruited and thus mimics sensory input into the brainstem, forming the auriculo-vagal afferent pathway (He, 2013). Because it projects the stimulus in the NTS, the auricular vagus nerve stimulation can modulate both autonomic nervous system and the central nervous system. The majority of vagus nerve afferent fibers such as those for visceral, taste, heart, and aorta, are connected to the nucleus of the solitary tract, while other afferents end in the nucleus spinalis of the trigeminal nerve, e.g., afferents for larynx and pharynx (Berthoud, 2000; Groves, 2005).

The activity of the vagus nerve plays a crucial role in several key functions (Trepel, 2017). It innervates the laryngeal muscles, allowing for proper breathing and speech. It also innervates the muscles of the pharynx and plays a role in taste in the pharynx and epiglottis area. Additionally, it plays a crucial role in respiratory regulation in the lungs and regulates the heart rate and blood pressure through innervation of the heart and aortic arch. As the largest parasympathetic nerve in the body and innervation of most viscera, it is natural to assume that the activity of the vagus nerve is closely associated with overall health and well-being. Studies have shown that decreased vagal function is negatively associated with morbidity, mortality, and psychological factors such as stress, depression, and anxiety (Thayer, 2009).

1.2 CLINICAL AND POTENTIAL USES OF VAGUS NERVE STIMULATION

Stimulation of the Vagus nerve has been used in epilepsy treatment since the early 1880s (Johnson RL, 2018). The stimulation takes places on the left cervical vagus nerve. This therapy proved very successful in treating refractory epilepsy and compared to drugs treatment leaves few side effects. Based on these side effects, it was concluded that vagus nerve activity influences numerous physiological activities. Following these conclusions, this therapy was slowly introduced in treating other conditions affected by the activity of the vagus nerve.

An overall mood improvement was observed therefore, the effects of vagus nerve stimulation were investigated on patients with depression. It was concluded that vagus nerve stimulation (VNS) offered a sustained symptomatic benefit after one year, but some additional, longitudinal, clinical studies, with larger patient cohorts are required (Duncan A. Groves, 2005).

At the same time, a reduction in anxiety was also observed. Even though this might possibly be a secondary effect of the treatment, the results were consistent with other reports of a therapeutic benefit

of VNS for anxiety. After a dedicated study, the patients reported improvement after 10 weeks of therapy (Duncan A. Groves, 2005).

Patients with depression were also reported to have a decreased sensation of pain. This led to the theory that VNS might be a viable treatment for inflammatory disorders associated with chronic of intermittent bouts of pain, such as fibromyalgia and migraines. In a migraine headaches study, 56% of the patients reported pain relief after 1 hour, while another study suggests that non-invasive VNS can be used to treat episodic cluster headaches (Johnson RL, 2018).

Treating some conditions is still under research, but the results prove that VNS can be used in many cases. A potential use was derived from epileptic patients, who experienced significant weight loss. Similar side effects were also present in patients with depression under VNS, who experienced attenuated food cravings. This led to studies on using the VNS in treating obesity. A study by Val-Laillet et al (2010) suggests that VNS does not actually cause weight loss, but instead prevents excess weight gain, by reducing the appetite (Johnson RL, 2018).

Another potential use for the vagus nerve stimulation is as an anti-inflammatory treatment. VNS may reduce the inflammatory response, activating the cholinergic anti-inflammatory system; a loop from the vagus afferents, through the autonomic brain stem, forebrain cortical structures, and through the descending vagus efferents (Johnson RL, 2018). Different studies focus on distinct aspects or conditions involving inflammation:

Sepsis progression was halted, by reducing inflammation through VNS which restored the equilibrium between parasympathetic and sympathetic tone (Johnson RL, 2018).

Atherosclerosis is believed to be caused by low-grade systemic inflammation; therefore, it is reasonable to use VNS in order to treat cardiac dysfunction and atherosclerosis. Sloan et al suggested in a CARDIA study that the vagus nerve stimulation is key to anti-inflammatory tone (Johnson RL, 2018).

Other studies and experiments showed that vagus nerve plays a significant role in pulmonary inflammation. VNS might also be useful in treating gut and lung injuries together, since it prevents intestinal barrier failure (Johnson RL, 2018).

Stroke and TBI could be alleviated with VNS, since they are caused by widespread neural inflammation. Because VNS has anti-inflammatory qualities and affects acetylcholine levels, these changes in cytokine upregulation and neurotransmitter balance may give an instantaneous and controllable means to manage harm caused by stroke, ischemia, or trauma (Johnson RL, 2018).

Since diabetes is another inflammatory-related disorder, VNS could be used as a treatment. Recent research has demonstrated the significance of the vagus nerve in the pathophysiology of diabetes and

other associated diseases, suggesting that VNS might be effective in treating such problems (Johnson RL, 2018).

1.3 Stimulation Methods

Vagus nerve can be stimulated in different ways. The first one was an invasive method, where surgery was required. The second method would be completely non-invasive, with surface electrodes. The third method is stimulating it through the auricular branch. This can be done non-invasive, or minimally invasive.

In an invasive VNS usually bipolar cuff electrodes are surgically implanted at the cervical level. The generator for these electrodes is usually implanted subcutaneously in the thoracic wall. This implantation is associated with high risks and costs, the electrodes implant is irreversible as well as infection-associated morbidity and surgical complications; cardiac arrhythmia under test stimulation and electrode malfunction are other risks (Spuck S, 2010). During treatment, other side effects appear, such as voice alteration, dysphagia, cough, swallowing difficulties, pain and in some patients even bradycardia (Elliott RE, 2011; Liporace, 2001).

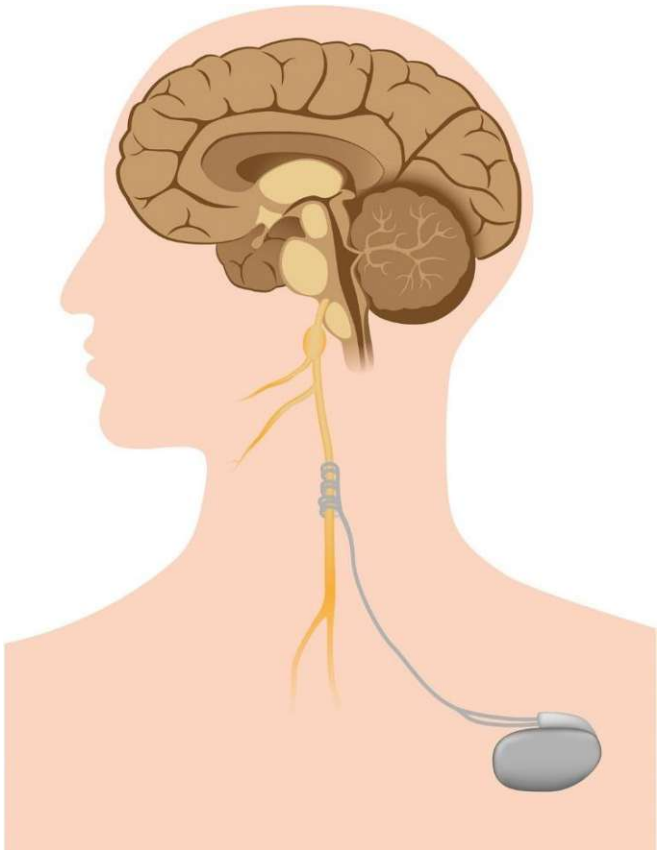

Figure 1.3.1 – Invasive, cervical vagus nerve stimulator.
(Onuora, 2016)

The vagus nerve can also be stimulated in a non-invasive manner. This method uses surface skin electrodes placed at the neck and stimulates the afferent branches of the cervical vagus nerve. The transcutaneous stimulation uses strong currents in order to circumvent the skin barrier. Electrical fields are created in the stimulation area, which leads to unwanted recruitment of efferent fibers and non-vagal nerves stimulation. Because of this side effects such as neck pain, dizziness, headache, nasopharyngitis, and oropharyngeal pain can appear (Gaul, 2016).

The vagus nerve can also be stimulated indirectly through its auricular branch. Transcutaneous auricular vagus nerve stimulation means that surface skin electrodes are places on the outer ear, which will then stimulate the receptive field of afferent auricular vagus nerve endings (Straube, 2015). Two electrodes are used in this stimulation and only afferent vagus nerve endings are stimulated. Still, if the surface electrodes are large, diffuse stimulation fields can form, stimulating non-vagal nerves as well. In order to circumvent the skin barrier of the ear and stimulate the regions innervated by auricular vagus nerve, good electrode contacts and strong currents are required. Transcutaneous auricular vagus nerve stimulation is safer than the invasive one and eliminates the risks, with mostly minor side effects such as headache, pain, and skin irritation at the stimulation site as well as dizziness (Badran, 2018b; Mertens, 2018).

By using miniature needle electrodes that penetrate the skin of the outer ear a percutaneous minimally invasive auricular vagus nerve stimulation can be achieved. This method usually uses two or three mini-needle electrodes (Kampusch, 2013). Because of the needle size, the stimulation fields are focussed and stimulates only afferent auricular vagus nerve endings. Also, because of the penetration of the skin, the contact impedance is lower and favours an energy efficient stimulation. This method also comes with minor side effects such as local skin irritation, local bleeding, pain at the stimulation site, and dizziness. Depending on the technique used to place the needles, local bleeding can be avoided (Roberts, 2016). Other side effects can rarely occur, and they appear due to afferent-efferent vagal reflexes with the vagal nucleus; examples are the Arnolds ear-cough reflex, ear-gag reflex, ear-lacrimation reflex, ear-syncope reflex, and Vaso-vagal reflex (Kaniusas, 2019).

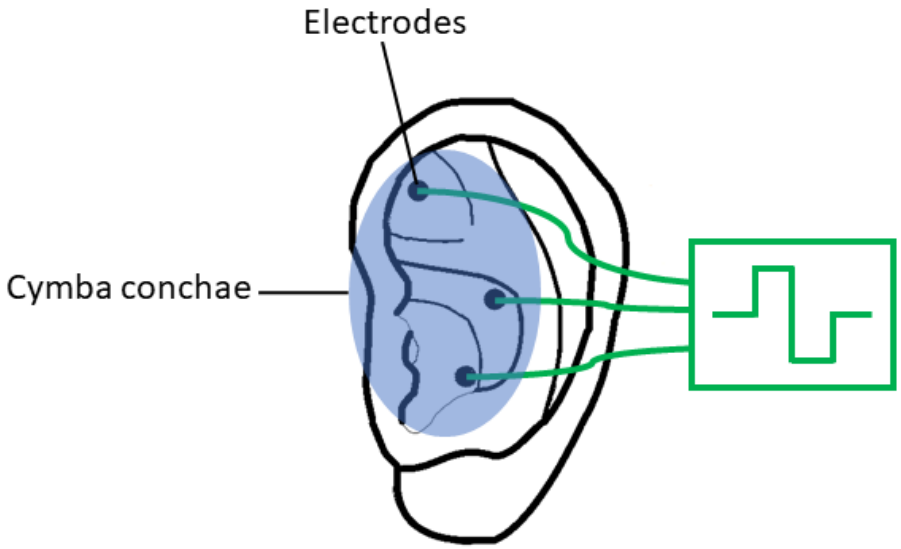

Figure 1.3.2 – aVNS electrode placement. Inspired from (Kaniusas, 2019)

Considering all the risks and side effects, it is safe to assume that non-invasive and minimally invasive stimulation methods yield fewer side effects, increasing the patients who could use such a treatment. The non-invasive methods are more cost effective, in comparison with the implantable devices, easy to apply and cannot recruit efferent vagus nerve fibers, eliminating a lot of other potential side effects. Through stimulation of the auricular vagus nerve certain functions of the brain can be modulated, increasing the therapeutic effect, and reducing the side effects (Kaniusas, 2019).

1.4 PERSONALIZATION OF VAGUS NERVE STIMULATION

There are many vagus nerve stimulators available. Most of them are simply preprogramed to stimulate at a certain frequency with a certain amplitude and cannot be modified. This is called for short open-loop stimulation. There are also closed-loop stimulators. These aim to improve the stimulation and adjust depending on the condition that is being treated and the patient.

An open-loop neuromodulation is a stimulator that is preprogramed to deliver a stimulus at a certain amplitude and with a certain frequency. According to Frei and Osorio (2001), vagus nerve stimulation yields different responses between patients, but consistent for each individual. Therefore, not adapting the stimulus in real-time in accordance with the bodily rhythms and momentary therapeutic needs may limit the stimulation effectiveness.

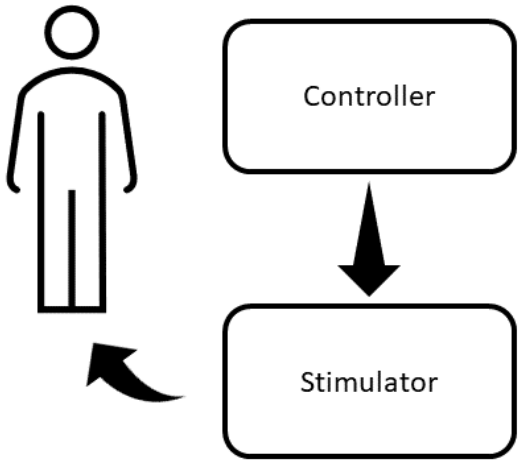

Figure 1.4.1 – Open loop Vagus nerve stimulation flow

Closed-loop neuromodulation aims to quickly adapt to the bodily rhythms, offering a personalized and effective therapy with increased efficiency. It minimizes clinical burden and offers the patient an increased quality of life and lower severity of side effects (Kaniusas, 2019; Stanslaski, 2012). Findings from Boon et al. (2015) show a reduction in seizure severity while using a closed-loop VNS. Another team showed that a closed-loop stimulation reduced the seizure frequency by 90%, while in the open-loop, the reduction was only 17% (Salam, 2015). Besides the clinical improvements, a considerate amount of energy can be saved with closed-loop stimulation (Grant, 2012).

Activation of the stimulator by the patient (e.g., via a button of magnet stick in response to upcoming pain) would close the loop. However, this closed loop is subjective and can only be applied in specific diseases such as chronic back pain. Also, in the absence of objective physiological data, patients cannot be expected to comply (Kampusch, 2016). Therefore, the stimulator must be activated or adjusted algorithmically utilizing various control models and individual physiological biofeedback. Closing the loop and enabling modification and customization of aVNS therapy is possible through the recording and analysis of various biosignals produced in response to aVNS.

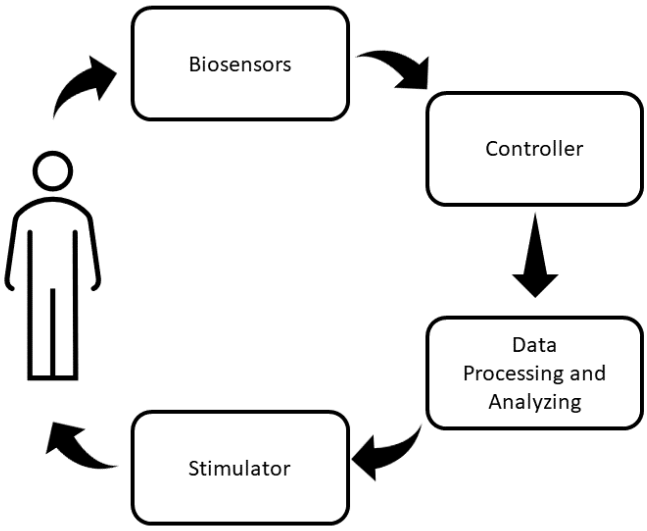

Figure 1.4.2 – Closed loop vagus nerve stimulation flow

The specific physiological signals used as biofeedback will depend on the aVNS's therapeutic or goal function. The biofeedback should contain detailed information in regard to the physiological reactions of the stimulation. Therefore, careful selection and specific processing of the biofeedback signal are essential. For example, when targeting peripheral vasodilation with VNS, peripheral blood flow can be used as a biofeedback signal; when targeting involuntary muscle contractions in dystonia, the tonus of the muscle excitation can be used; electrocardiogram can be used for detecting stressful pain attacks or suppressing atrial fibrillation (Boon, 2016).

2 METHODS

To create a closed-loop VNS the use of a biosignals is mandatory. The monitoring bio-signal is chosen based on the application. The heart activity is however monitored regardless of the application, due to the fact that the effects of the stimulation are observed almost immediately in the activity of the heart.

Studies have showed that the timing of the stimulation in correlation with the inner body rhythms, such as heart activity and respiration, are of high relevance and can deliver a more efficient treatment (Brown, 1934). Sclocco et al. (2019) have shown that stimulation during exhalation enhances engagement of key neuromodulator brainstem nuclei as well as increasing the stimulus-evoked cardiovagal outflow.

Taking all of this into consideration the most appropriate biosignals to monitor is firstly, the electrical heart activity (ECG) and on the second plan the respiration activity, which can be easily recorded through chest bioimpedance.

Table 2.1.4 – Materials used for this work

Physical device	
Biosensor	MAX30001
Microcontroller	Nucleo-G474RE
BIOPAC	MP36
Software	
STM32 MXCube	Version 6.5.0
STM32 CubeIDE	Version 1.9.0
MATLAB + Simulink	Version 2022a
RealTerm	Version 3.0.1.43

2.1 BIO-SENSORS

The key technology used to develop the system is the biosensor. Since the parasympathetic nervous system regulates the heart rate, pulse, blood pressure, and respiration, via the vagus nerve, the best bio-signal to be acquired would be ECG. All sensors compared for this purpose can therefore acquire ECG signal. Sensor selection is depended on features such as, accuracy, energy consumption, communication protocol, filtering, and size.

Table 2.1.1 – Sensor feature comparison

Manufacturer		Analog Devices	Texas Instruments	Maxim Integrated	Maxim Integrated
Model no.		AD8233	AFE 4900	MAX86150	MAX30001
Supply voltage	V	3.6	1.8/2 & 1.8 & 5	1.8 & 3.3	1.8 & 3.3
Supply current	µA	50	≲600	≲750	≲232
Filters		Not integrated Two-pole High-pass Three-pole low-pass	Decimation filter	High-pass filter Digital low-pass filter	Digital High-pass filter, Digital low-pass filter
Communication		Analog	I2C, SPI	I2C	SPI
Bio-signal		Bio-potential	Bio-potential, PPG, SPO2	Bio-potential, PPG, SPO2	Bio-potential, Bio-impedance
Sample resolution			24 bits for ECG	18-bit for ECG	18-bit for ECG
Other Features					Dedicated hardware for R-to-R detection

The AD8233 is the perfect solution to quickly measure the raw bio-potential data. It has the possibility of implementing low-pass and high-pass filter to remove noise and motion artifacts, but the standard chip does not come equipped with such filters. The output of the chip is analogue, which means an analog-digital converter is needed before the microcontroller can process and analyse the data. Integrated in the chip are a couple very useful features, such as:

Adjusting the cut-off frequency automatically after a sudden change in the signal, such as removing the leads. This enables the sensor to record valid data quickly after the electrodes are reconnected.

Right leg drive (RLD) amplifier. This improves the common-mode rejection of the line frequencies and other interferences.

The supply current is typically 50 µA, making the chip very low power.

The AD8233 is an integrated signal conditioning block for measuring biopotential. It can implement a low-pass filter as well as a high-pass filter, for motion artifacts. The cut-off frequency is automatically adjusted to a higher filter to quickly recover after a sudden signal change, such as a leads-off condition, allowing the sensor to record valid data quickly after the electrodes are reconnected.

The output signal of the AD8233 is an analog signal, unfiltered signal. This signal needs first to be discretised and then filtered in order to reduce the noise. This constitutes a big disadvantage compared to other sensors, because this conversion requires more resources from the microcontroller, slowing down the entire process of acquisition and analysis.

The TI sensor outputs a digital signal. A decimation filter integrated is used to down sample the discrete signal to the desired sampling rate. It does integrate an ADC noise reduction algorithm. It can communicate through serial protocol interface (SPI) which can be at high speeds reducing the overall latency and it also has a high sample resolution with a big storage capacity. It can acquire two types of bio-signals: ECG and Photoplethysmography (PPG) through the later being able to measure the oxygenation of the blood as well.

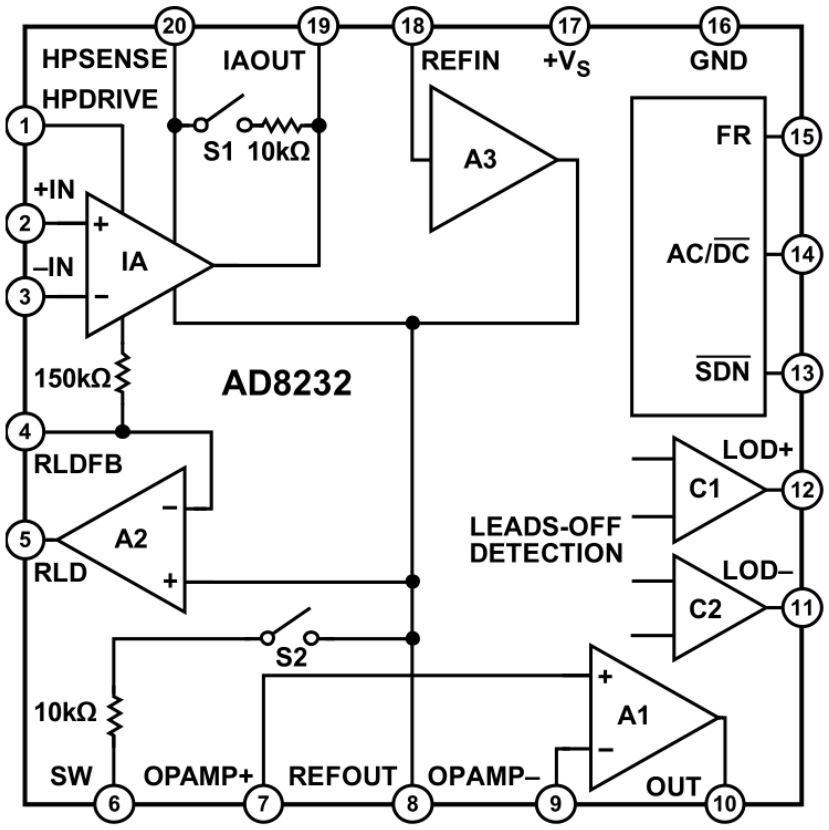

Figure 2.1.1 – AD8232 schematic (Analog Devices, 2020).

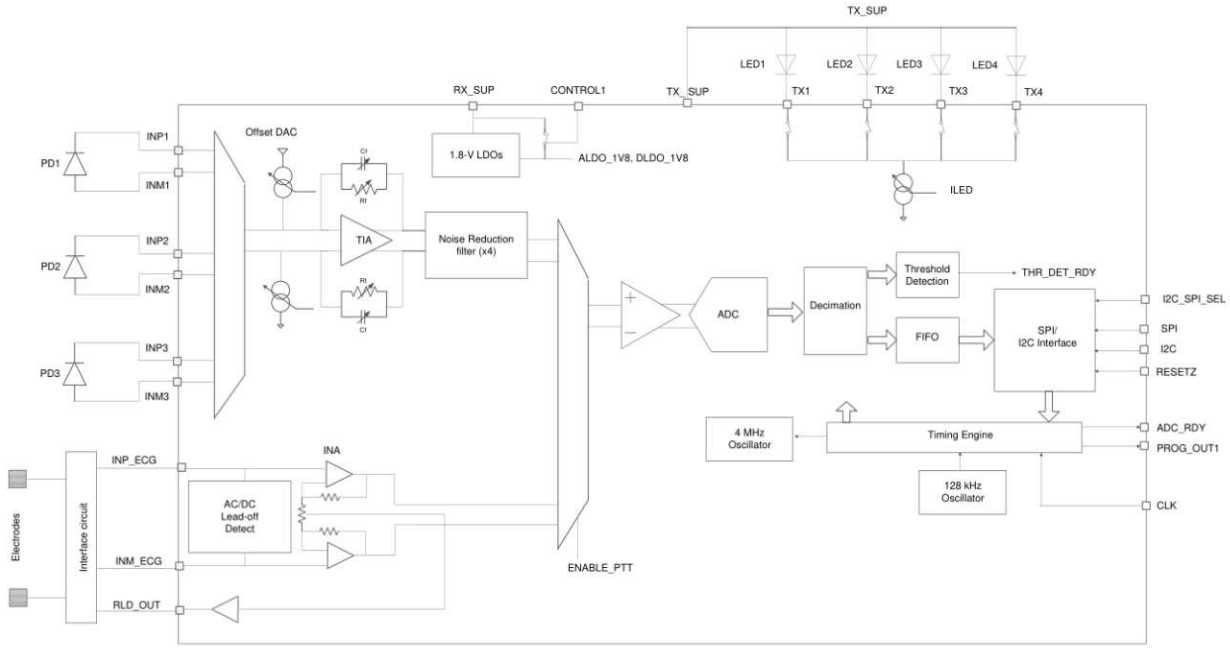

Figure 2.1.2 – Texas Instrumens AFE 4900 schematic (Texas Instruments, 2017)

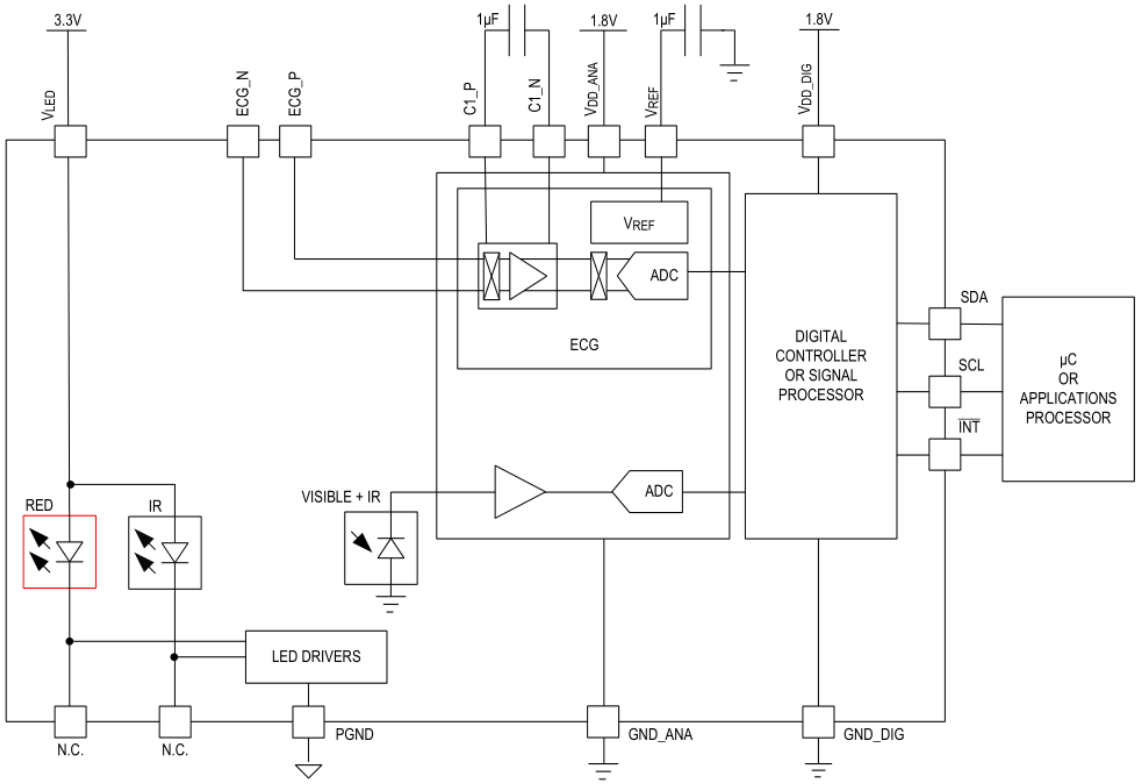

Figure 2.1.3 – MaximIntegrated MAX86150 schematic (Maxim Integrated, 2016)

On the downside it needs extra hardware for the proper power supply. Depending on the configuration the power consumption can be quite high without the possibility to integrate any filter on the acquired signal. This implies that the microcontroller will have to pre-process the signal before it can be analysed.

MAX86150 has can consume more power than the TI sensor, but that depends on the configuration. Another disadvantage is the communication protocol, which is slower than the SPI. It can also acquire two types of bio-signals: ECG and Ppulse plethysmography (PPG) through the later being able to measure the oxygenation of the blood as well. MAX86150 integrates a high-pass filter as well as a digital low-pass filter, removing the strong radiofrequencies, common-mode line frequency, movement artifacts, and other electrical noise. The ADC offers an 18-bit resolution for the ECG signal.

Out of all the proposed sensors, MAX30001 is the only one that has a clinical-grade ECG, as well as BioZ analog front end with high resolution data converter and is compliant with the international standard for ambulatory electrocardiographic systems.

Just as MAX86150 our chosen sensor, MAX30001 also offers an 18-bit resolution for the ECG signal, and instead of the PPG module, the MAX30001 has a bio-impedance module, which is very useful in directly measuring the respiration, with the same pair of electrodes with which ECG is measured. It integrates programmable digital low-pass and digital high-pass filters, and it has a built-in heart rate detection, eliminating the need to run a heart rate algorithm on the microcontroller. MAX30001 consumes less power than both AFE4900 and MAX86150, at most, depending on the configuration. It communicates with the microcontroller through SPI at speeds as high as 12 MHz. Both the biopotential and bioimpedance channels feature extensive calibration voltages for built-in self-test.

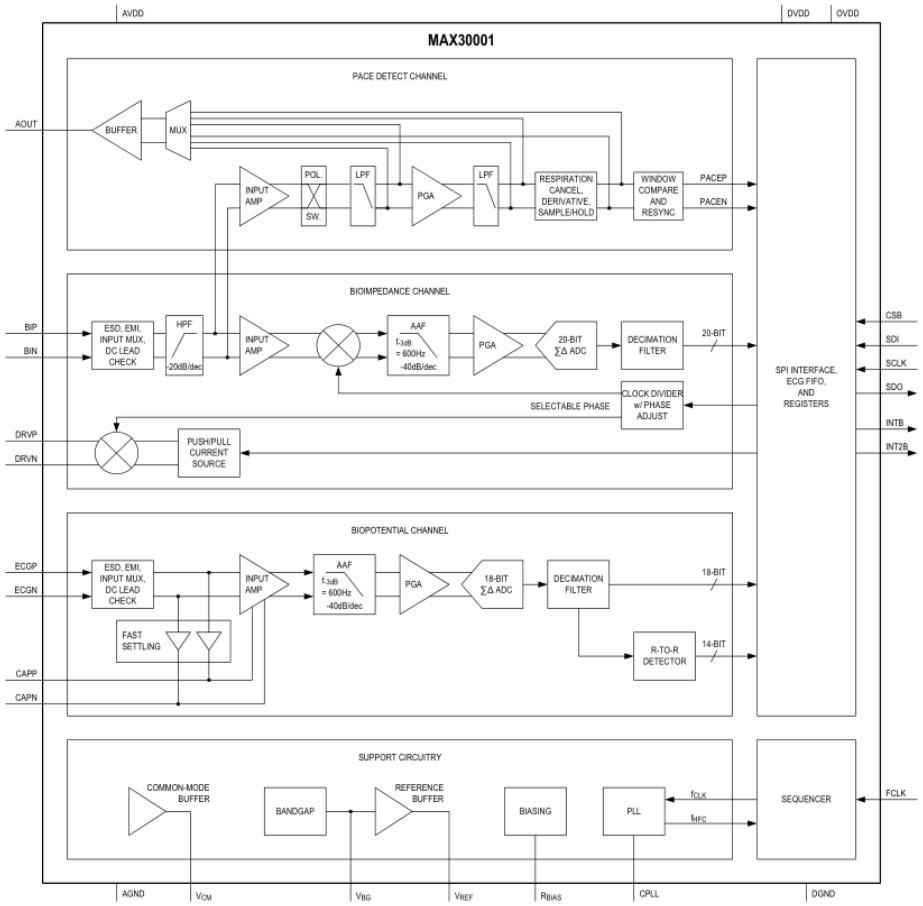

Figure 2.1.4 - MaximIntegrated MAX30001 schematic (Maxim Integrated, 2019)

2.2 MICROCONTROLLER

The main system of the closed-loop feedback device includes the microcontroller and the biosensor. A microcontroller is an integrated circuit chip that contains a processing core, internal memory, various peripherals, and the capability to execute predefined instructions to achieve control of externally connected devices and storage of data for processing. The microcontroller will control the entire system by interfacing with the biosensor and later with the stimulator, control data collection, trigger and adapt the stimulation, save data, and maintain system operation. For such an application, the microcontroller requires: I/O ports, SPI to support the sensor, UART/USART to send data/receive data, analog-to-digital conversion, low power capability, timing functionality, external and internal memory for permanent and temporary storage.

There are multiple microcontrollers available from many vendors (e.g., Texas Instruments, Microchip, STMicroelectronics, etc.), but due to its versatility, inter-series compatibility, ultra-low power performance, the high-performance Arm® Cortex®-M4 32-bit RISC core and the fact that it is already used for the stimulator, STM LQFP64 is one of the best suited microcontrollers for this application (STMicroelectronics, 2022).

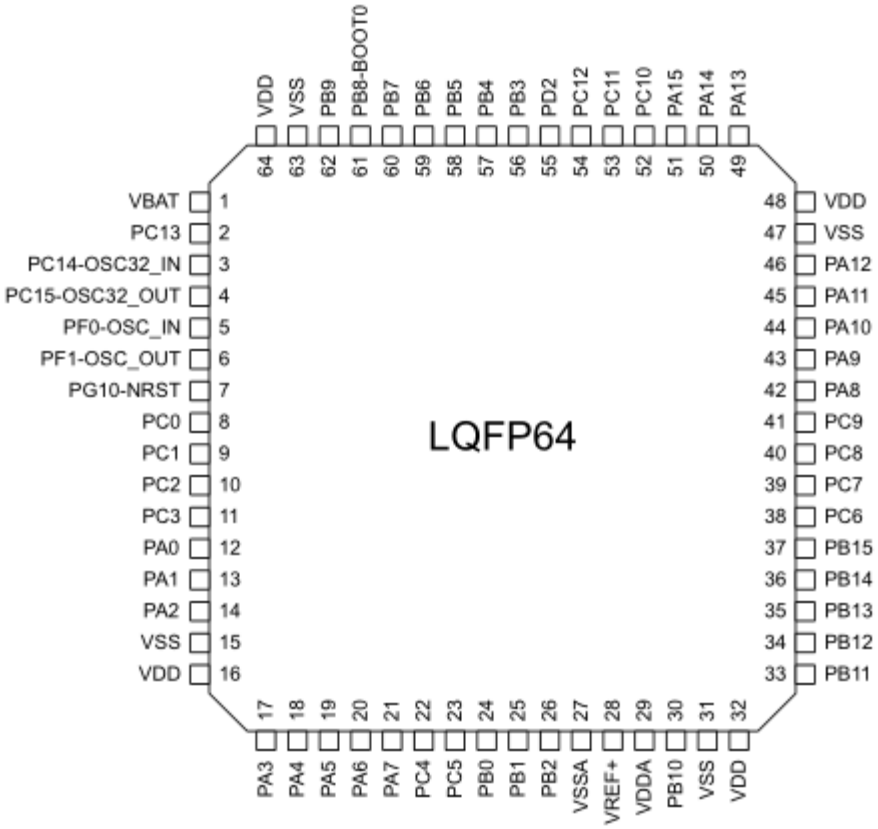

Figure 2.2.1 – STM LQFP64 microcontroller chip pinout (STMicroelectronics, 2021).

This device has a high-speed memory (512 Kbytes of Flash memory, and 128 Kbytes of SRAM), an extensive range of enhanced I/Os, 12-bit ADCs, a low power RTC, various timers. The LQFP64 is also integrated in some development kits such as Nucleo-G474RE, which offer a straightforward way to use the module for testing and debugging.

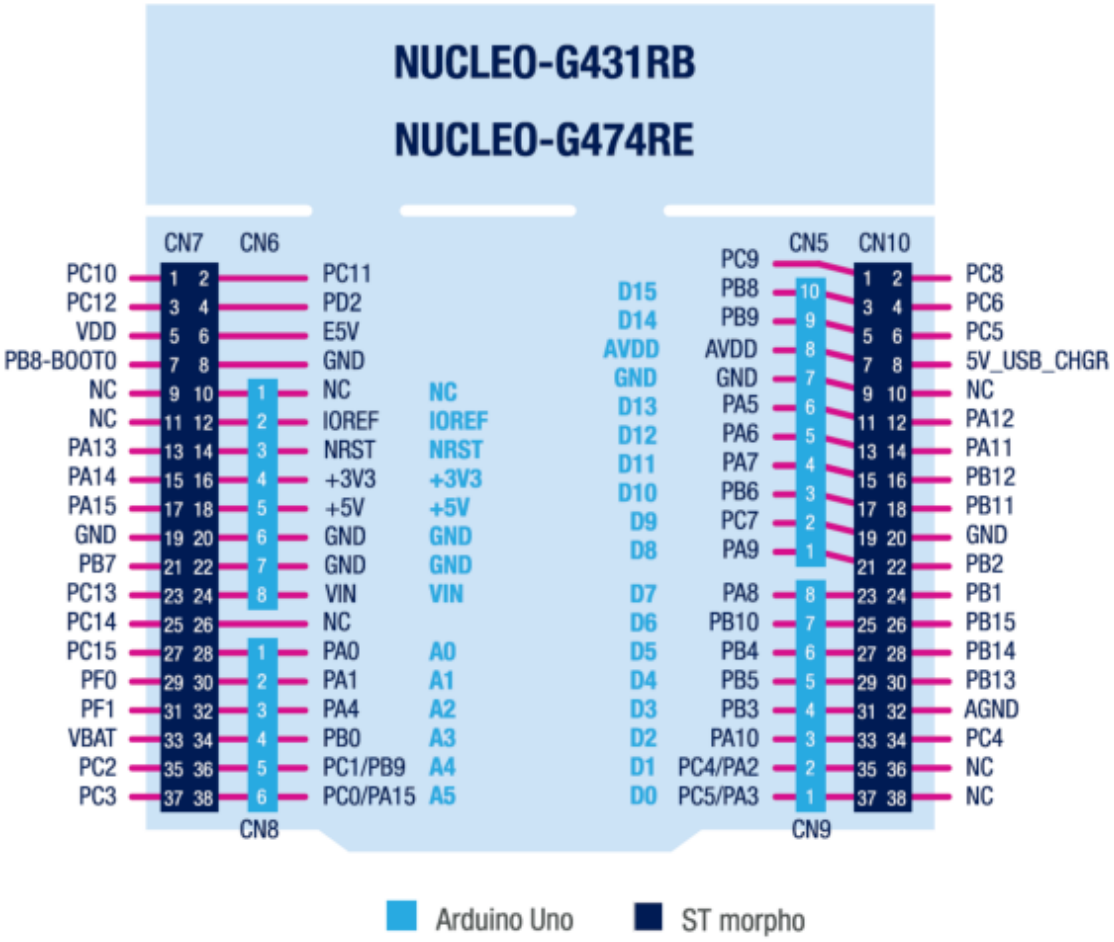

Figure 2.2.2 – STM32 Nucleo-G431RE development board pinout (STMicroelectronics, 2019).

STM also offers free software development tools such as CubeMX and CubeIDE.

CubeMX is a software developed by the STMicroelectronics in order to help developers in reducing development of time, effort, and cost. CubeMX is a visual tool for configuring STM32 microcontrollers and microprocessors and generating the corresponding initialization code in C. It contains a database of STM32 microcontrollers, peripherals, and middleware.

First step is to select the microprocessor or microcontroller or a development board. After this the user needs to configure the clock tree (clock sources, prescaler and frequency values). If the user uses invalid settings or there are some conflicts in the configuration, CubeMX proposes a solution that is remarkably close to the user's configuration. Now, the user can start configuring peripherals such as GPIO pins, communication protocols (UART/USART, SPI, I2C or CAN), timers, ADCs, DACs, or various embedded systems.

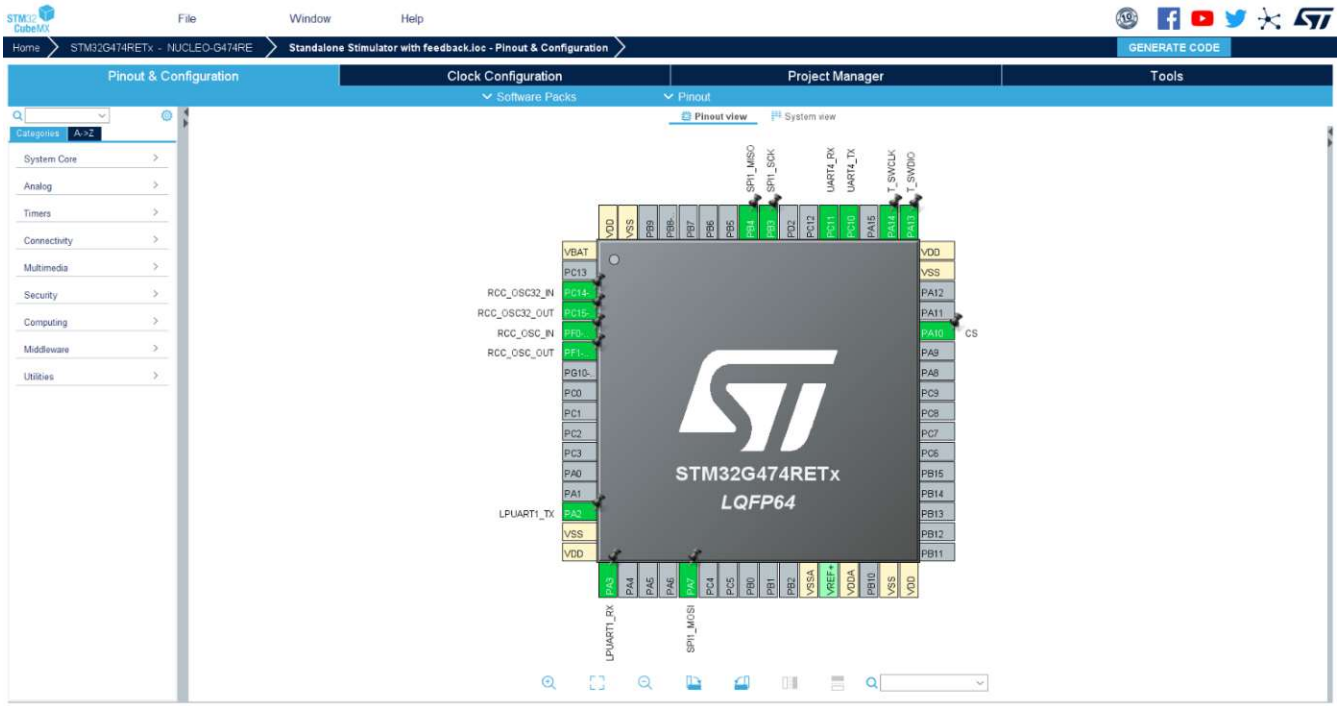

Figure 2.2.3 – STM CubeMX software. Show the pin configuration of the microcontroller

Once the user has finished configuring the microcontroller according to the use application, the initialization C code can be generated and is ready to be used within several development environments. The generated C code is based on STM32Cube HAL firmware libraries and only covers peripheral and middleware initialization, which use the drivers included in STM32Cube.

CubeIDE is a C/C++ development platform that includes peripheral configuration, code generation, code compilation, linking, and debugging capabilities. It is based on the Eclipse/CDT framework and GCC toolchain for development, and GDB for the debugging.

2.4 MATLAB AND SIMULINK

MATLAB stands for MATrix LABoratory. It is a software package used by engineers and scientists to analyze data develop algorithms and create various system models. MATLAB uses a high-level programming language that expresses matrix and array mathematics directly. It also provides toolboxes from signal and image processing, control systems, wireless communications, computational finance to robotics, deep learning, and AI, and much more. This vast library of toolboxes can be further expanded with packages and toolboxes shared on GitHub, MATLAB File Exchange, and other platforms.

MATLAB also includes pre-built applications, and the user can also create new applications with graphical user interface (GUI), which then can be deployed on cloud and enterprise systems or converted to C/C++, HDL and CUDA code to run on embedded devices.

Simulink is a block diagram environment for designing multidomain models, simulating before migrating to hardware and deploying without writing code. It can be used to model multidomain systems and simulate how all the system's components behave. The models are created using block diagrams, which help understanding and analyzing complicated systems.

A wide range of analog, digital, mixed-signal, and multi-rate systems can be simulated, and then scaled up to hundreds of simulation parameters. The performance of the algorithm can also be monitored as it adapts to match the necessary requirements. Simulink also provides add-ons to extend the capabilities of the model-based design, allowing integration of complicated logic, accountability of latency and other network impact. The model can also be enhanced by using specific tools to controls, signal processing and communications applications. The final model may be used to automatically create code for real-time prototyping and testing, as well as deployment on an embedded device.

As a result of Simulink's integration with MATLAB, the analysis can be expanded, simulation automated, and it has the benefit of utilizing alternative parameters for the models, or simply execute MATLAB code within the model.

2.5 REALTERM SERIAL MONITOR

RealTerm is a software designated specifically for receiving or sending not just ASCII data, but also long sequences of binary, hexadecimal, or decimal values. The software has a terminal window, where it displays the received data and a menu where the port to be monitored or through which data is sent can be configured. The data can be displayed in multiple formats such as ASCII, ANSI, Hexadecimal, Binary, Float, integer, or unsigned integer up to 16 bits. It also offers options to log the data, as well as timestamping the data in different formats.

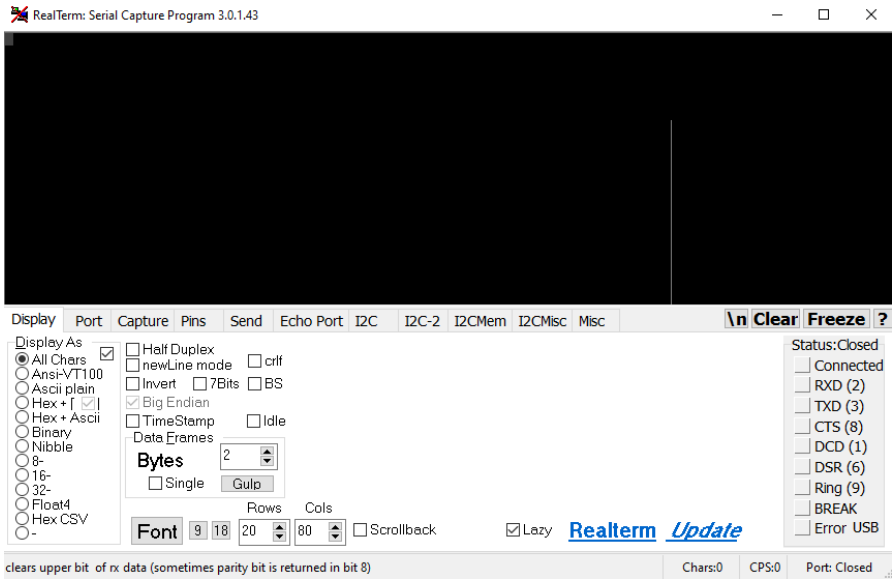

Figure 2.5.1 – RealTerm serial monitor software.

2.6 BIOPAC SYSTEM

BIOPAC MP36R is a data acquisition system for life science research. The system has built-in universal amplifiers that can record a wide range of physiological signals, a stimulator, audio output, external trigger, and digital I/O lines. The system is also capable of gas and airflow analysis and supports both wireless and wired signal-specific amplifiers. It comes with a dedicated software with which automated analysis routines for ECG, HRV, EEG, EMG, EGG, and others can be done. The MP36R system is approved for both human and animal research, and when used together with AcqKnowledge software, BIOPAC electrodes, transducers, and other system components, is part of a complete data acquisition and analysis system.

Figure 2.6.1 – BIOPAC MP36R device (BIOPAC, 2022).

2.7 Functional Validation of MAX30001

A sensor evaluation or development board that provides a single platform for evaluating a sensor's or design's capabilities and functioning. The MAX30001EVSYS development board includes the MAX30001 and a MAX32630FTHR Cortex-M4F, which contains a firmware to allow a smooth communication with a dedicated graphical user interface (GUI) software provided by Maxim Integrated. This evaluation board also includes all circuitry necessary for powering the system, as well as test points, and jumpers to configure different functionalities of the sensor.

The development board helped in the progress of this thesis by providing an intuitive GUI software in which the sensor can be configured, assessed, and even make recordings. Even though all the necessary details were provided in the datasheet, this external validation helped in understanding the inner workings of the sensor.

The MAX30001 has many features that can be configured for ECG, HR detection and Bioimpedance, which can be seen in Figure 2.7.2. The configurable features for ECG include channel gain settings, sample rate, digital high-pass filter and digital low-pass filter cutoff frequency.

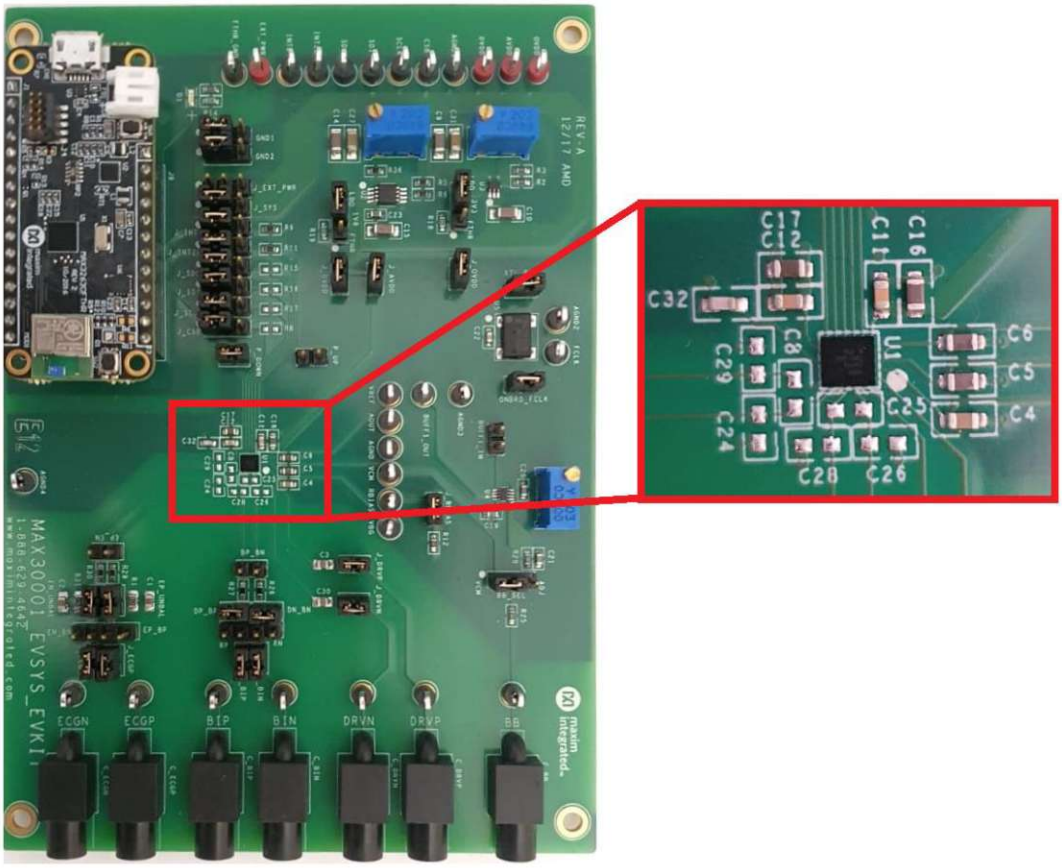

Figure 2.7.1 – MAX30001EVSYS – evaluation kit for MAX30001. Focus on the MAX30001 chipset.

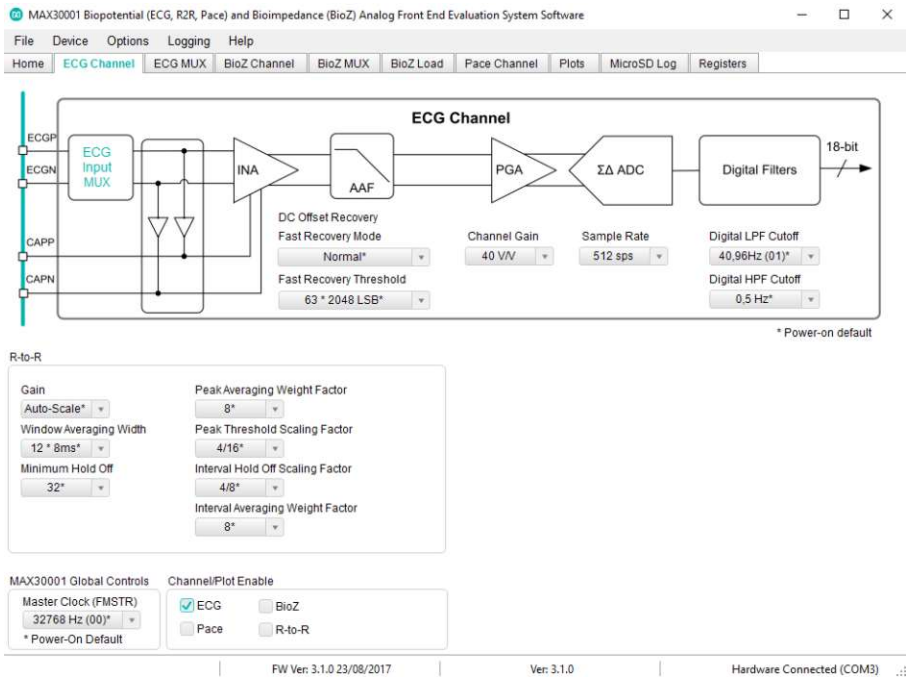

Figure 2.7.2 – MAX30001 evaluation kit GUI. In the figure the settings for the ECG channel can be seen..

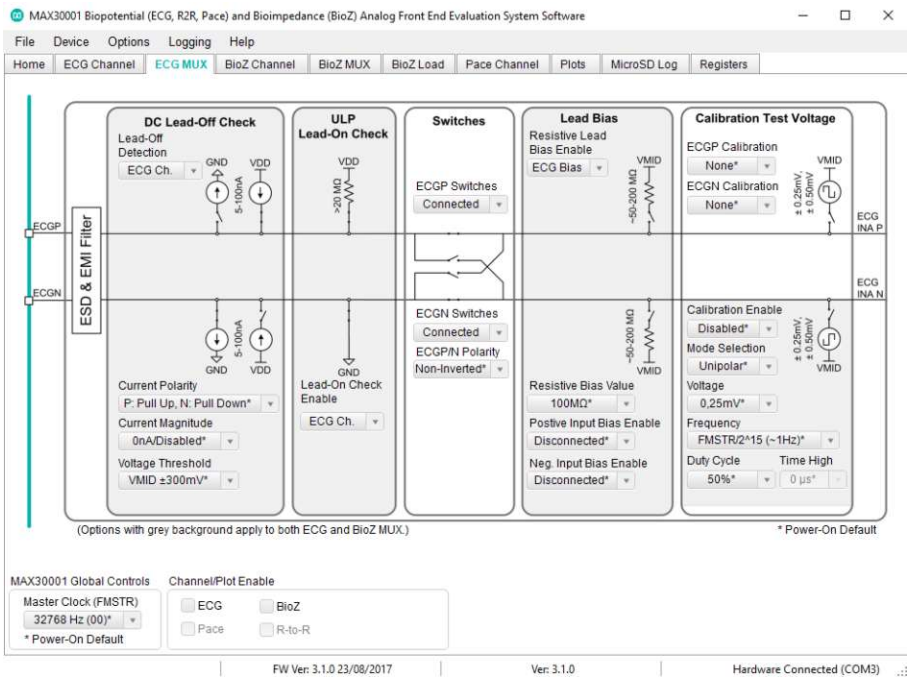

Figure 2.7.3 – MAX30001 evaluation kit GUI. This figure shows the ECG MUX settings.

To record data from a patient, the electrodes have to be placed a certain way. The electrodes can be places either on the chest, as in Figure 2.7.4 A, or on the arms and foot, as in Figure 2.7.4 B. The red electrode should be connected to the positive input, according to the electrical schematic (Figure 2.7.5). The blue electrode should be connected to the negative input. The black electrode should always be connected to the body bias drive. In the case the white and red electrode are inversely connected, the configuration can be changed to internally reverse them. In case this is not corrected in the configuration, the system might fail to detect the R-peaks, or it will identify Q- or S-peaks as R-peaks.

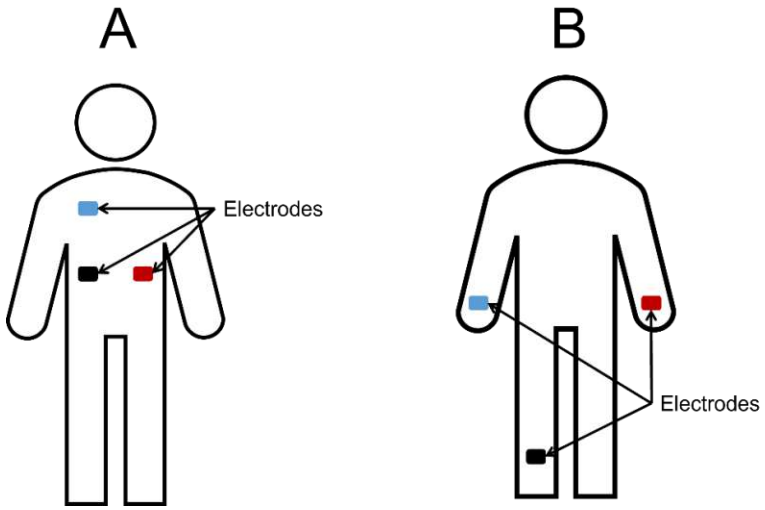

Figure 2.7.4 – Electrode placement for ECG recording. A – chest placement; B – Arms and right leg placement. Blue – negative electrode; Red – positive electrode; Black – body bias drive.

Figure 2.7.5 shows the electrical schematic of the MAX30001. Since MAX30001 has three supply voltage requirements (OVDD, AVDD, DVDD), each corresponding to the logic interface, analog circuitry and digital circuitry voltage, the schematic also presents the necessary circuitry for the power supply (excluded) and the electrodes connectivity. The analog and digital circuitry require 1.8 V volts, while the logic interface needs 3.3 V. By already using 3.3V at the interface level, it removes the need for extra circuitry to be able to communicate with external devices at a higher supply voltage than 1.8V. MAX30001 and LQFP64 communicate using the SPI protocol; this requires that the LQFP64 controls this communication channel. The SPI communications signals can have different abbreviations or names, depending on the manufacturer and developer. In the schematic, on MAX30001, CSB, SCLK, SDI, and SDO appear, and they are connected to CS, SCLK, MOSI and MISO; these abbreviations correspond to chip select, clock, slave data in or master out slave in, slave data out or master in slave out. The interface and specific pins connected between these two devices for SPI communication are summarized in Table 2.7.1.

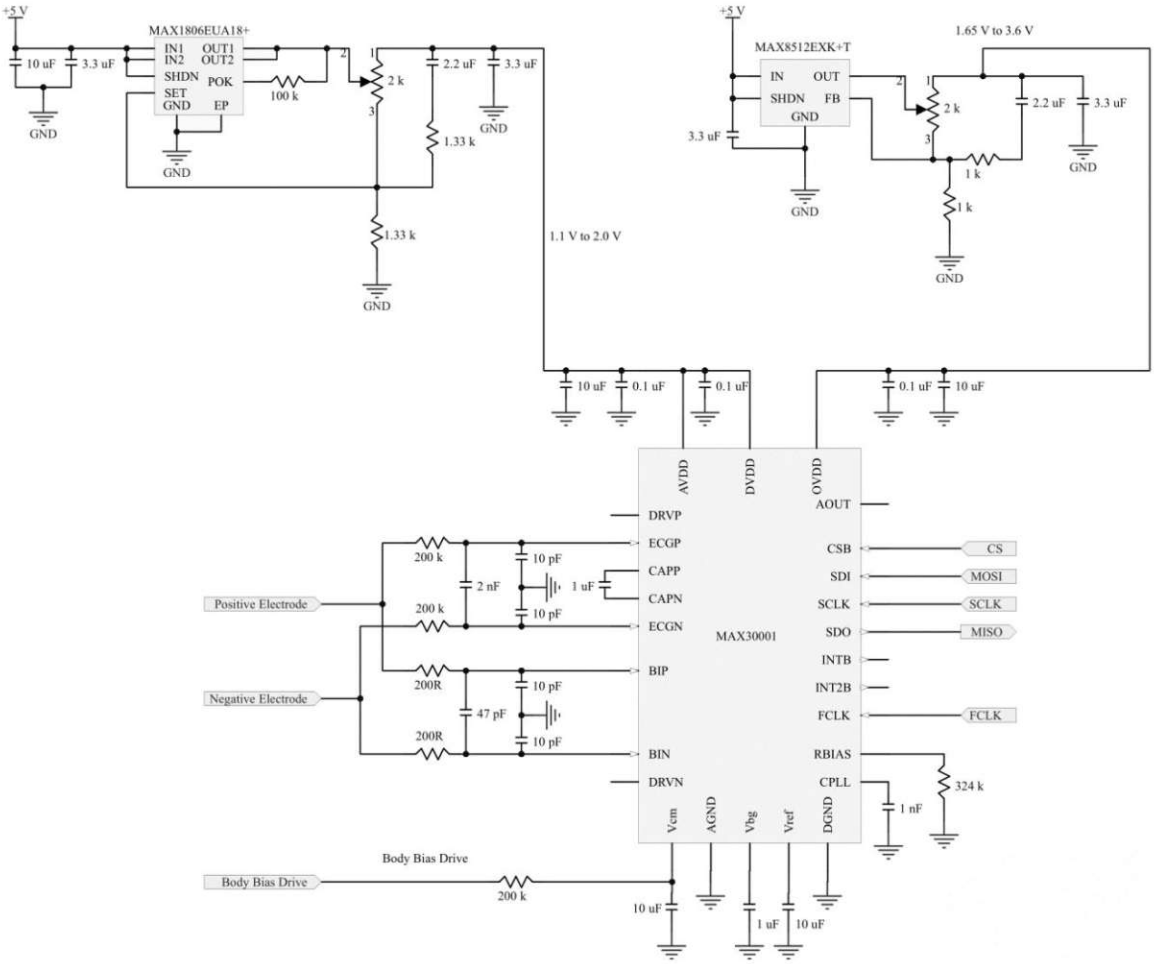

Figure 2.7.5 – MAX30001 electrical schematic with power supply elements.

Table 2.7.1 – Pin configuration for SPI communication

MAX30001 Pins	LQFP64 Pins
CS	PA10
SCLK	PB3
SDI	PA7
SDO	PB4

In order to configure the SPI protocol on the LQFP64, the first thing that needs to be done is to set the peripheral clock frequency and the baudrate prescaler in order to get a value that falls in the MAX30001s range. After this the clock polarity and the clock edge must be set accordingly as well as the frame format, bits order, and number of data bits. For all of these, the datasheet of MAX30001 and a couple of tests were particularly useful.

As mentioned earlier the GUI interface, proved to be especially useful in establishing communication between the LQFP64 and MAX30001. The registers tab from the GUI offers a comprehensive overview of the registers and their values at a specific point. The values obtained through the GUI, were cross checked with the preliminary values obtained with the LQFP64. The reading settings on the LQFP64 were adjusted until the values of certain registers, such as the INFO and EN_INT registers matched. After this, a write function was implemented in an equivalent manner.

Before programming the system, a series of configuration function were written and then assessed. These functions were defined in a library used in the main program of the system and were only called during the initialization phase. Once these configuration functions were assessed, a preliminary Read ECG function was also developed. A set of preliminary tests and comparisons of the configurations and acquired signal were conducted between this system and the MAX30001 GUI.

In order to get the real values of the acquired ECG data, the raw data had to be converted using a formula provided in the datasheet. This formula is presented in the Equation (2.7.1) and uses the following parameters: ADC value, the ADC reference voltage (V_{REF}), and the value of the gain (ECG_GAIN). Before this conversion could be made, the raw data had to be extracted from the four bytes received from the MAX30001. The structure of the received raw data can be seen in Figure 2.7.6. The three bits ETAG are used as an ECG data tag and show in what mode was the data acquired and its validity. The three bits representing the PTAG show if an ECG FIFO sample has related PACE information. This tag stores a pointer to the appropriate location within the PACE FIFO where the PACE information is stored. After the removal of these tags, the eighteen bits corresponding to the raw ECG value are concatenated in one variable and converted to a signed magnitude, which can then be used in Equation (2.7.1).

REG	FIFO AND MODE	DATA STRUCTURE (D[23:0])																							
		23	22	21	20	19	18	17	16	15	14	13	12	11	10	9	8	7	6	5	4	3	2	1	0
0x20	ECG Burst	ECG Sample Voltage Data [17:0]																		ETAG [2:0]			PTAG [2:0]		
0x21	ECG	ECG Sample Voltage Data [17:0]																		ETAG [2:0]			PTAG [2:0]		
		23	22	21	20	19	18	17	16	15	14	13	12	11	10	9	8	7	6	5	4	3	2	1	0

Figure 2.7.6 – MAX30001 internal FIFO structure (Maxim Integrated, 2019).

$$V_{\mathrm{ECG}}\,(mV) = \frac{ADC \times V_{\mathrm{REF}}}{2^{17} \times ECG\_GAIN} \tag{2.7.1}$$

3 RESULTS

3.1 IMPLEMENTATION WITH STM LQFP64

The block diagram in Figure 3.1.1 provides a high-level understanding of system operation. First step would be to initialize the internal clocks on STM LQFP64 to control overall microcontroller speed and communication protocol speeds. During the initialization phase of system operation, the LQFP64 configures the MAX30001 using the SPI.

The second step is to initialize all the communication protocols, in order to communicate with the sensor, as well as with an external device. Next step is to initialize the sensor (MAX30001) with the predefined configuration. For the sensor configuration, multiple functions were programmed, but not before creating a library with all the registers names and addresses.

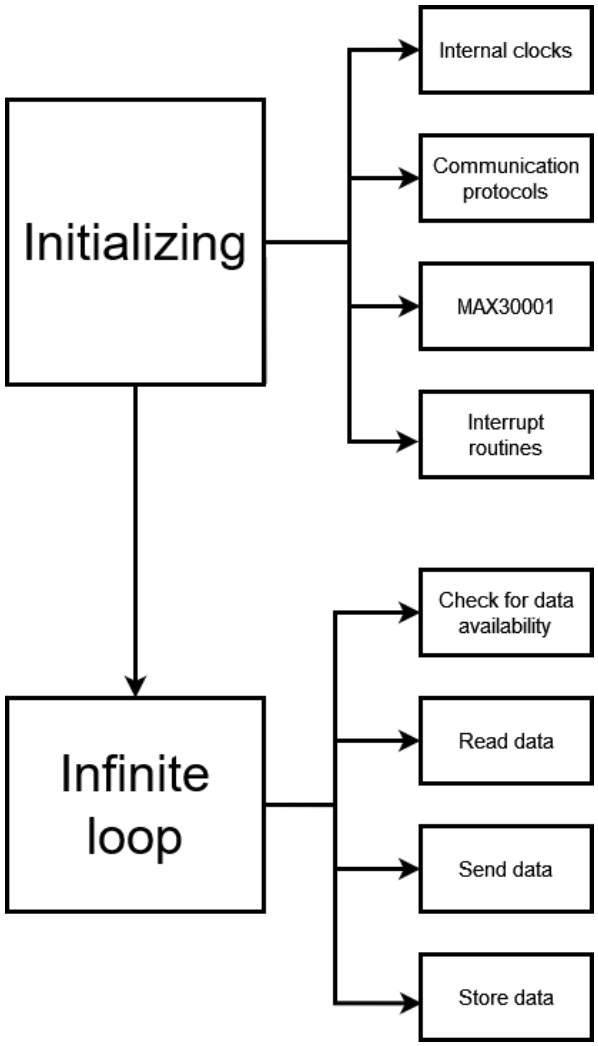

Figure 3.1.1 – High level flow diagram of the program.

To make the configuration of the sensor easier and faster, designated functions were developed. They all follow a similar flow, which is presented in Figure 3.1.2. This flow is repeated for all the registers that need to be changed to achieve the desired configuration.

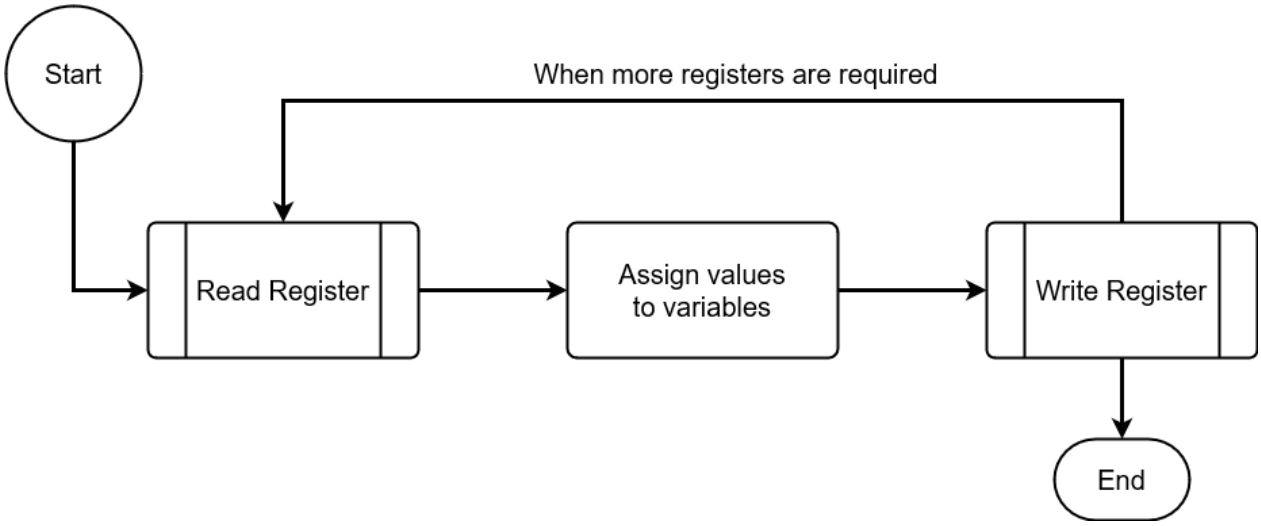

Figure 3.1.2 – MAX30001 configuration function flow diagram.

The registers used by LQFP64 to configure the ECG functionality and the description of each register can be seen in Table 3.1.1. The MAX30001 datasheet contains information on the exact register configurations enabled by these instructions (MaximIntegrated, 2019). Table 3.1.2 shows the possible configurations for the sensor.

Table 3.1.1 – Registers used to configure the ECG channel

Register Name (Address)	Brief description
CNFG_GEN (0x10)	General settings
CNFG_EMUX (0x14)	Configures ECG MUX settings
CNFG_ECG (0x15)	Configures ECG settings
MNGR_INT (0x04)	Interrupt Manager
SYNCH (0x09)	Starts new ECG operation

Table 3.1.2 – All possible configurations for the ECG channel

Register	Default	Description and values
En_ecg	0	ECG Channel Enable
		0 = ECG Channel disabled
		1 = ECG Channel enabled
Openp	1	Open the ECGP Input Switch (most often used for testing and calibration)
		0 = ECGP is internally connected to the ECG AFE Channel
		1 = ECGP is internally isolated from the ECG AFE Channel
Openn	1	Open the ECGN Input Switch (most often used for testing and calibration)
		0 = ECGN is internally connected to the ECG AFE Channel
		1 = ECGN is internally isolated from the ECG AFE Channel
Pol	0	ECG Input Polarity Selection
		0 = Non-inverted
		1 = Inverted
Calp_sel	00	ECGP Calibration Selection
		00 = No calibration signal applied
		01 = Input is connected to VMID
		10 = Input is connected to VCALP (only available if CAL_EN_VCAL = 1)
		11 = Input is connected to VCALN (only available if CAL_EN_VCAL = 1)
Caln_sel	00	ECGN Calibration Selection
		00 = No calibration signal applied
		01 = Input is connected to VMID
		10 = Input is connected to VCALP (only available if CAL_EN_VCAL = 1)
		11 = Input is connected to VCALN (only available if CAL_EN_VCAL = 1)
E_fit	01111	ECG FIFO Interrupt Threshold
		00000 to 11111 = 1 to 32
Rate	10	ECG Data Rate (also dependent on FMSTR selection, see CNFG_GEN Table 33):

		FMSTR = 00: fMSTR = 32768Hz, tRES = 15.26µs (512Hz ECG progressions)
		00 = 512sps
		01 = 256sps
		10 = 128sps
		FMSTR = 01: fMSTR = 32000Hz, tRES = 15.63µs (500Hz ECG progressions)
		00 = 500sps
		01 = 250sps
		10 = 125sps
		FMSTR = 10: fMSTR = 32000Hz, tRES = 15.63µs (200Hz ECG progressions)
		10 = 200sps
		FMSTR = 11: fMSTR = 31968Hz, tRES = 15.64µs (199.8Hz ECG progressions)
		10 = 199.8sps
Gain	00	ECG Channel Gain Setting
		00 = 20V/V
		01 = 40V/V
		10 = 80V/V
		11 = 160V/V
Dhpf	1	ECG Channel Digital High-Pass Filter Cutoff Frequency
		0 = Bypass (DC)
		1 = 0.50Hz
Dlpf	01	ECG Channel Digital Low-Pass Filter Cutoff Frequency
		00 = Bypass (Decimation only, no FIR filter applied)
		01 = approximately 40Hz (Except for 125 and 128sps settings, see Table 33)
		10 = approximately 100Hz (Available for 512, 256, 500, and 250sps ECG Rate selections only)
		11 = approximately 150Hz (Available for 512 and 500sps ECG Rate selections only)

Interrupt routines must also be defined and initialized before starting the main program. The interrupt routines allow the normal flow of the program to be interrupted at any moment in order to process an event in a timely manner. In this work, one external interrupt was used so that the sensor could interrupt the normal flow to mark a new R-peak. A second external interrupt was used during the simulation process to mark the beginning of a stimulation event. Figure 3.1.3 shows how the interrupts are managed.

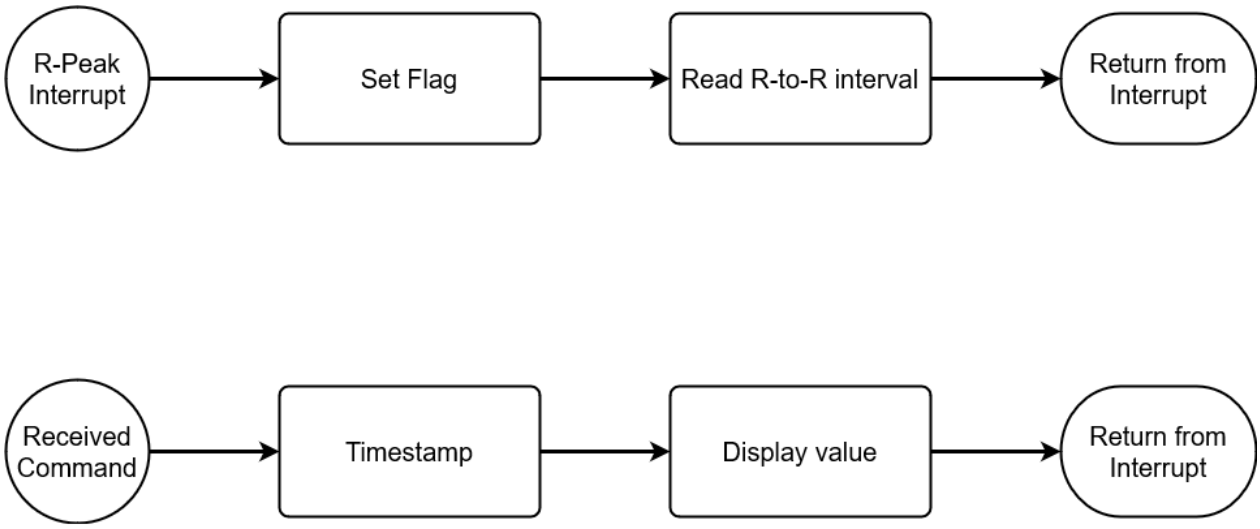

Figure 3.1.3 – Interrupts function flow diagram

After the initialization is complete, the program enters a continuous loop. In this continuous loop, the program will read the status register of the sensor every time the loop restarts. The status register offers a comprehensive overview of the current state of the sensor. Next the program will check the status register if there is a FIFO memory overflow. If an overflow was detected, the FIFO memory will be reset, otherwise the program will move to the next step.

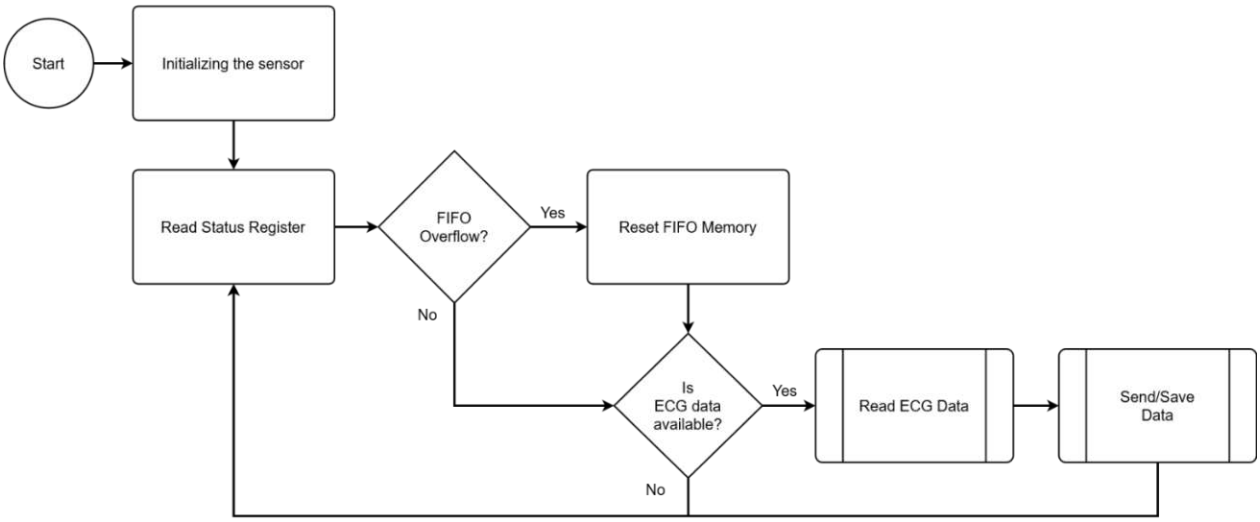

Figure 3.1.4 – Main loop flow diagram

The third step in this loop is to verify the STATUS register if ECG data is available in the FIFO memory. When data is available, the program will jump in the Read ECG data function. Once the reading is complete, it will jump back in the main loop and save the data in the Flash memory or send it to the PC. After this, the loop will restart. In case there is no ECG data available, the loop will simply restart and read the status register again. This sequence of events can be stopped at any time by the one of the interrupt routines as explained earlier.

Figure 3.1.5 presents the functionality of the Read ECG Data function. The data is firstly read from the sensor through SPI communication. The received data is split into three bytes (24 bits). From these three bytes, ETAG (3 bits) and PTAG (3 bits) are extracted. The ETAG value is used to determine if the read value is valid or not. Once the validity of the data is proven, the remaining eighteen bits, representing the ECG voltage value, are concatenated in a single variable. In a separate variable the timestamp of the sample is added. Both the timestamp and the sample value are stored in a temporary memory, until it is either saved in the Flash memory, an external memory, or sent to a different device. The sequence of events detailed above, is repeated until the length of the FIFO memory has been read completely.

To avoid any misinterpretation of acquired data and to have full knowledge of when an event occurred, a timestamp needs to be linked to each acquired sample. The real time clock module integrated in the Nucleo32 development board was used to solve this issue. First, a clock source had to be chosen from the clock tree (Figure 3.1.6). After enabling the real time clock, a starting data and time was provided.

The provided time is the starting point from which the real time clock will start counting, during the initialization phase. Due to the rather complicated timestamp structure, a timestamp conversion function was developed. This function would convert the timestamp to Unix format, providing an easy to manage and transfer value for the timestamp.

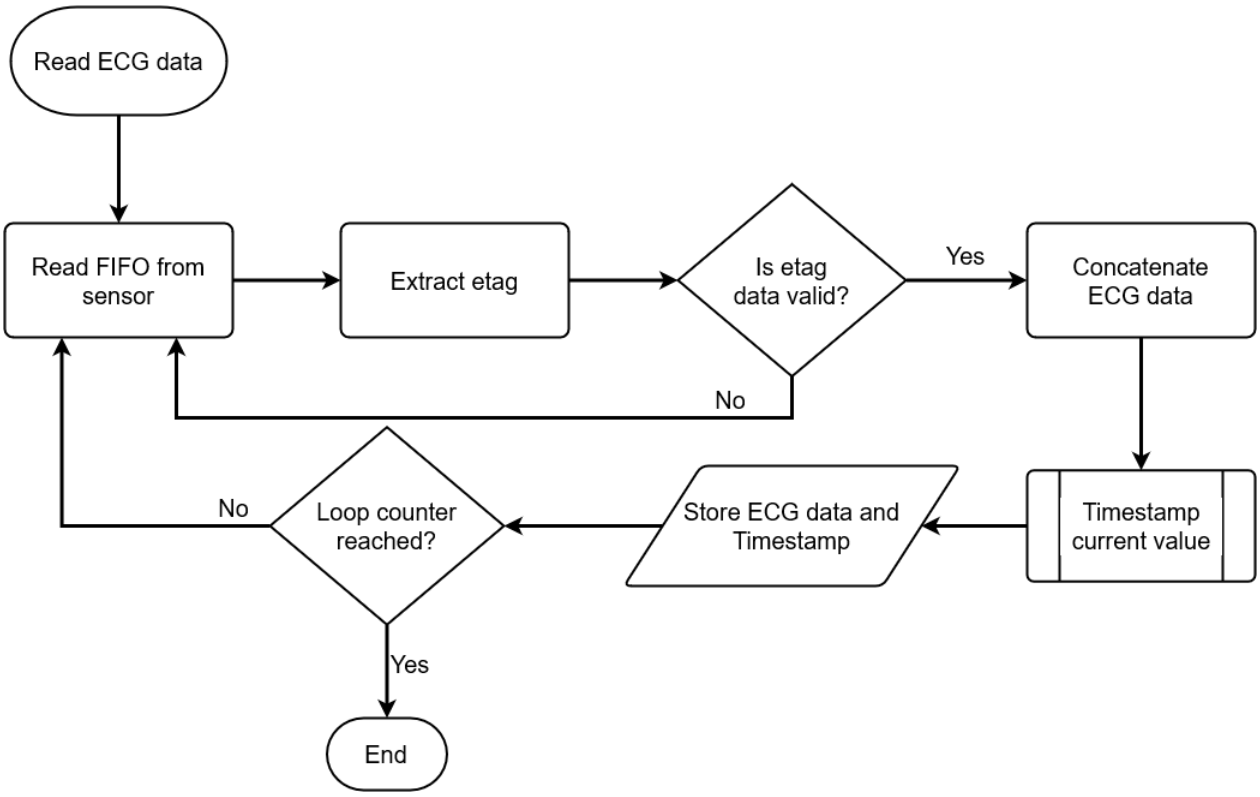

Figure 3.1.5 – ECG read function flow diagram.

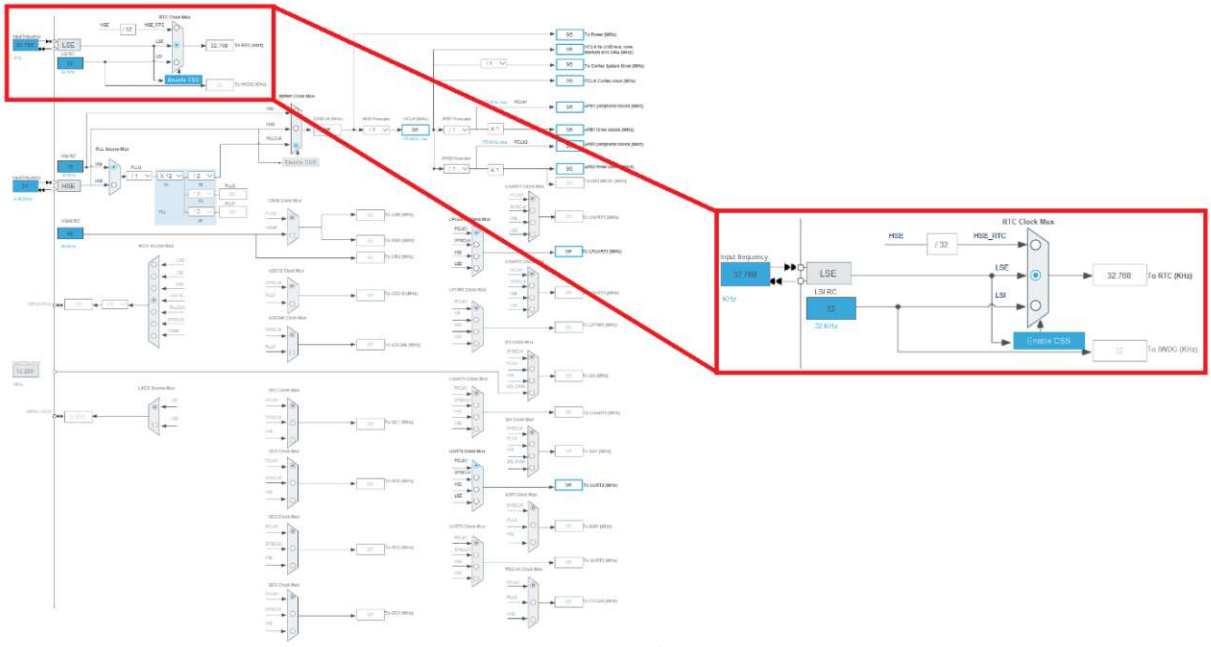

Figure 3.1.6 – LQFP64 clock tree diagram with focus on the Real Time clock (RTC) sources and configuration

Table 3.1.3 – Native Timestamp structures

Time Structure		
	Hours	0 - 12
	Minutes	0 - 59
	Seconds	0 - 59
	TimeFormat	AM/PM
	SubSeconds	Time unit range between [0-1] Second
	SecondFration	Synchronous pre-scaler
	DayLightSaving	Unused
	StoreOperation	Unused
Date Structure		
	WeekDay	1 - 7
	Month	1 - 12
	Date	1 - 31
	Year	0 - 99

The native format of the timestamp generated by the RTC is split in two structures, one for date and one for Time (Table 3.1.3). To converted into Unix format the values for, year, month, date, hours, minutes, and seconds were extracted from the native structures and put in a single structure. This new structure was then converted into Unix timestamp using mktime command.

As seen in Table 6 the native timestamp structure does not have the number of milliseconds directly. Using equation (3.1.1) the milliseconds value was calculated.

The Unix timestamp is in general expressed in seconds. Therefore, the milliseconds were added to the timestamp using Equation (3.1.2).

$$Miliseconds = \frac{(SecondsFration - Subseconds) \times 1000}{SecondsFraction + 1} \quad (3.1.1)$$

$$Timestamp = 1000 \times unixTimestamp + miliseconds \quad (3.1.2)$$

Sending the data from the microcontroller to the PC required another serial connection. The protocol for this was UART. An FTDI interface was required in order to connect the microcontroller to the PCs USB port. The FTDI adapter module, enabled a proper "conversion" from the UART port to the USB port. The UART protocol was set up in the microcontroller according to Table 3.1.4.

Table 3.1.4 – UART communication protocol configuration

Baud Rate	115200 Bits/s
Word Length (including Parity)	8 Bits
Parity	None
Stop Bits	1

Receiving the data on the PC required the configuration of the specific USB or serial port to be configured with the same settings as in the microcontroller (Table 3.1.4). All data coming through the serial port could be seen using a serial monitor such as RealTerm, or after assessing the connection, recording it in MATLAB. For this, MATLAB had to identify the same header value sent from the microcontroller, and then start recording the actual data.

Sending the data from the microcontroller followed these steps (Figure 3.1.7): in a buffer variable, the ECG value was added, then the timestamp of said value; next a header value was sent through the UART protocol, after which the buffer variable containing the actual data was sent.

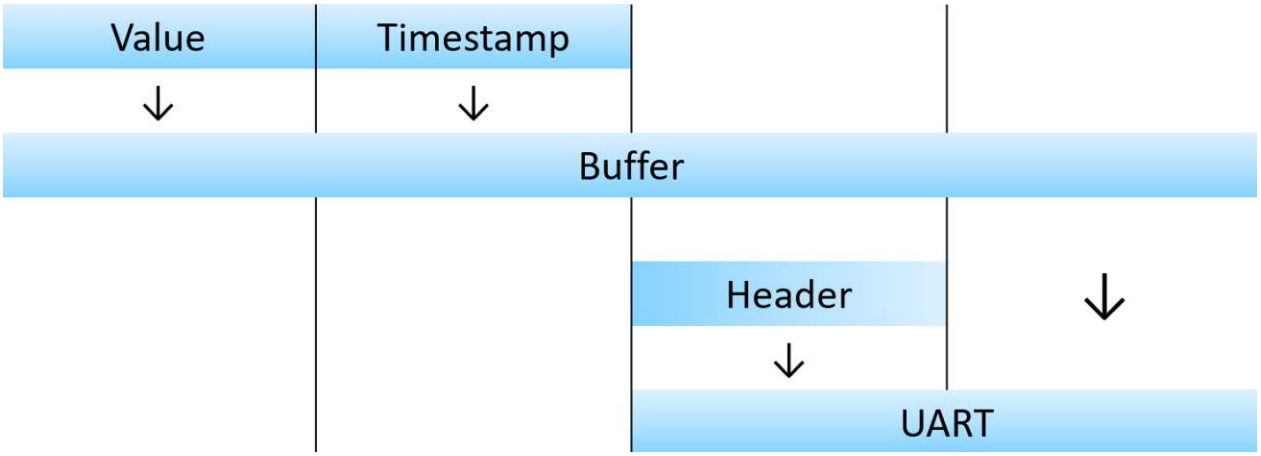

Figure 3.1.7 - The flow of sending data from the microcontroller

Saving the data for post analysis, required a PC to which the data was sent. Since this work is aimed at an independent device, for preliminary tests, the internal Flash memory was used. The Flash memory's structure as seen in Figure 3.1.8, is split into two banks and 256 pages. Since the first bank is used for the firmware, the data would be saved in the second bank. Due to the size of this bank, only recordings of 30 to 40 seconds could be stored, as each sample had both a voltage or raw value and a timestamp. The structure of the Flash memory only allows doublewords – 64 bits values can be written in the flash memory. Equation (3.1.3) describes how the data was packed to form a doubleword.

Flash area		Flash memory addresses	Size (bytes)	Name
Main memory (512/256/128 KB)	Bank 1 (256/128/64 KB)	0x0800 0000 - 0x0800 07FF	2 K	Page 0
		0x0800 0800 - 0x0800 0FFF	2 K	Page 1
		0x0800 1000 - 0x0800 17FF	2 K	Page 2
		0x0800 1800 - 0x0800 1FFF	2 K	Page 3
		-	-	-
		-	-	-
		-	-	-
		-	-	-
		0x0803 F800 - 0x0803 FFFF	2 K	Page 127
	Bank 2 (256/128/64 KB)	0x0804 0000 - 0x0804 07FF	2 K	Page 0
		0x0804 0800 - 0x0804 0FFF	2 K	Page 1
		0x0804 1000 - 0x0804 17FF	2 K	Page 2
		0x0804 1800 - 0x0804 1FFF	2 K	Page 3
		-	-	-
		-	-	-
		-	-	-
		-	-	-
		0x0807 F800 - 0x0807 FFFF	2 K	Page 127

Figure 3.1.8 – Internal structure of the Flash memory of LQFP64

$$Packed = Value \times 10^9 + Timestamp \tag{3.1.3}$$

The data stored in the Flash memory had to be unpacked in order to distinguish between the timestamp and ECG value. Unpacking meant that the entire value is divided by 10^9 and save the remainder as the timestamp, while the quotient is the voltage value. It is simply the reverse of the (3.1.3). Before writing any data in the flash memory, the second bank of it, had to be erased, to avoid data corruption during writing or reading from the flash memory.

To evaluate this process of data storage, the data recorded was stored, but also sent to the PC and stored in comma-separated values (CSV) file. At the end of the recording, the data stored in the microcontrollers internal Flash memory, was also sent to the PC. In MATLAB, the Flash memory data was compared to the data saved on the PC during the recording.

3.2 INTEGRATION WITH MATLAB

MATLAB was used to record, analyse, compare, and visualize the data. In order to achieve communication between the microcontroller and MATLAB, a serial port protocol had to be established. The serial port feature allows the user to configure the serial communication, by choosing the port, setting the baudrate, parity, number of bits that represent one character of data, stop bits, byte order, and other properties. The configuration used for receiving data is the same one presented in section 3.1 Table 3.1.4 ; all the extra configurable features for the serial port were left in their default mode.

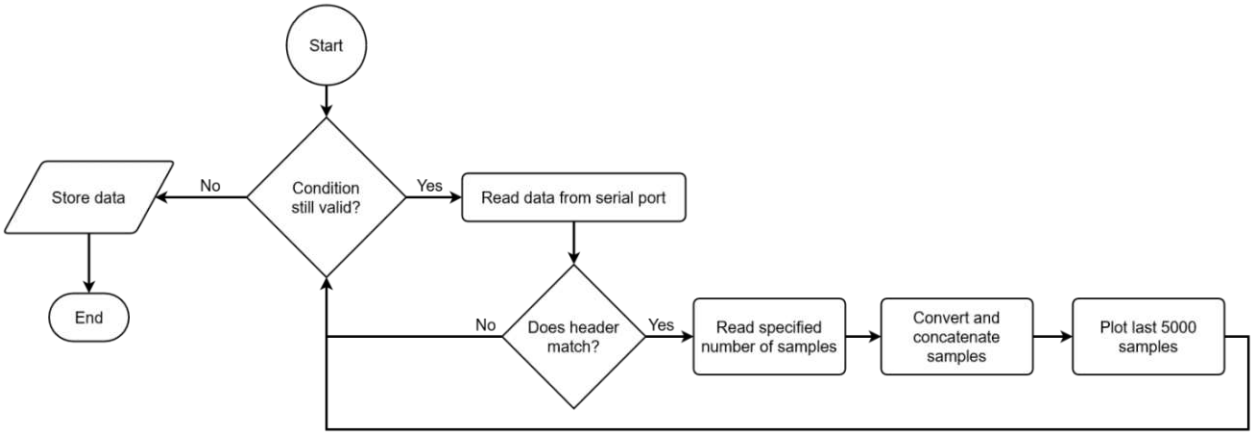

Figure 3.2.1 – MATLAB program flow diagram

The function to read data from the serial port has the following parameters: serial port object, number of samples, and data type. Since data were sent in sets of ten samples, each beginning of a set was marked with a header. The program would read values from the serial port and compare each one to the predefined header until a match would be found. Once the beginning of the data set was found, the next ten values read would be further processed in the program.

At first, every sample would be converted to a signed magnitude form and then concatenated in a data array. If timestamps were also sent, they had to be converted in MATLAB timestamp format, for easier handling. After these conversions, the data would be plotted for evaluation, saved in a file for later analysis, or both.

In the testing phase, two versions of the program were made, one that would record data for a specified amount of time, and one that would record for a specified number of samples. Both of these versions would follow the same flow as the one presented in Figure 3.2.1.

For an easier evaluation of the data and with an almost instantaneously feedback of the recording, a "real time" plot was developed. Since MATLABs purpose is not to be an embedded development environment, it takes some time to read the data from the serial port and to plot it. These two factors add up to a few milliseconds of delay between the time an event occurred and the time it is displayed in the plot. This delay is not relevant for a simply visual aid in the development process.

The algorithm of this plot is as follows: it plots every data point, over and over, until the number of samples reaches 5000. After 5000 samples, it only plots the last 5000 samples. This number was chosen, based on the sample rate set in the sensor, and is the equivalent of 10 seconds of recording. In this manner, the "real time" plot will have a moving window, showing only the last 10 seconds of the recording, except for the first 10 seconds. Once the recording is finished, all the data is saved in a file for future analysis.

Different configurations of the sensor were evaluated. Figure 3.2.2 shows the results of one of the first configurations, while Figure 3.2.4 shows one of the best configurations for ECG data acquisition.

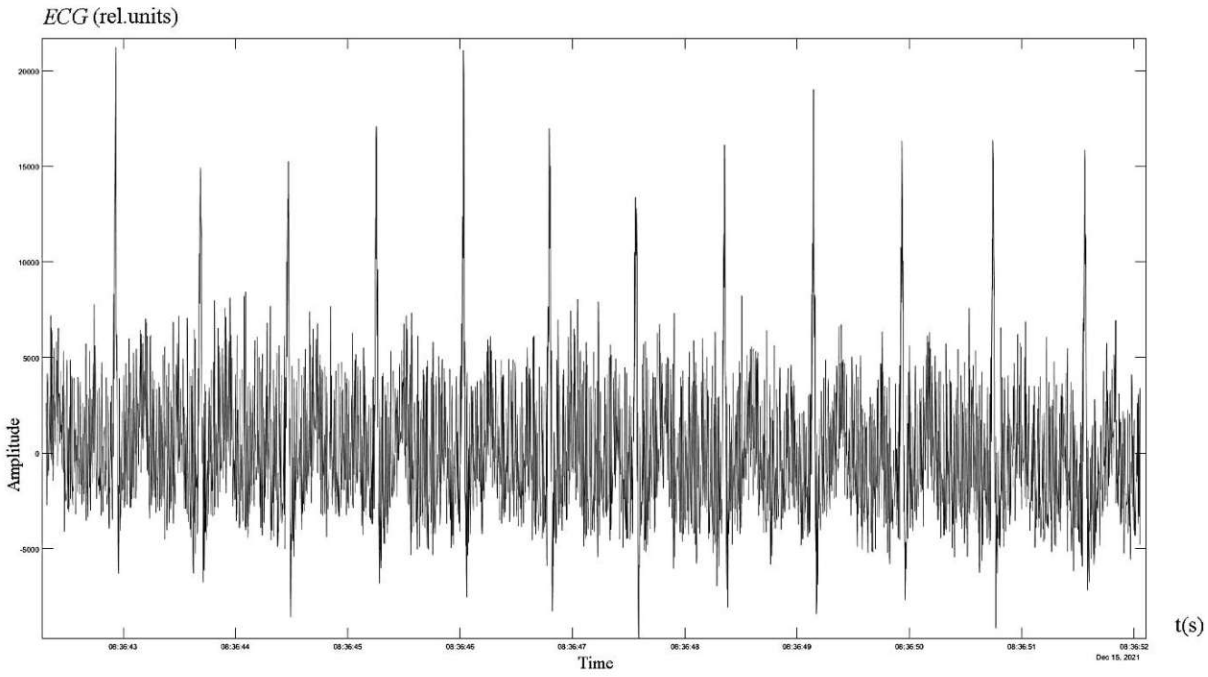

Figure 3.2.2 – Ten seconds windows of an ECG recording with MAX30001 without using the digital filters.

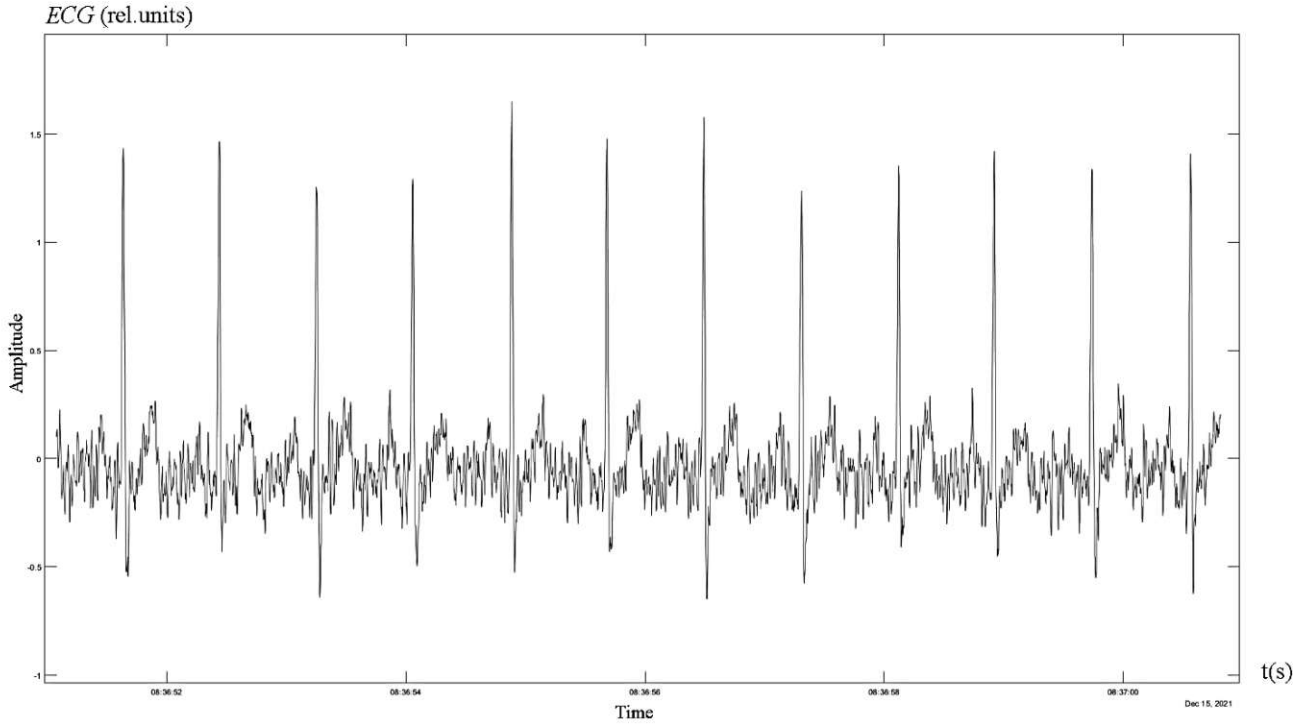

Figure.3.2.3 – Ten seconds windows of an ECG recording with MAX30001 with digital filters activated.

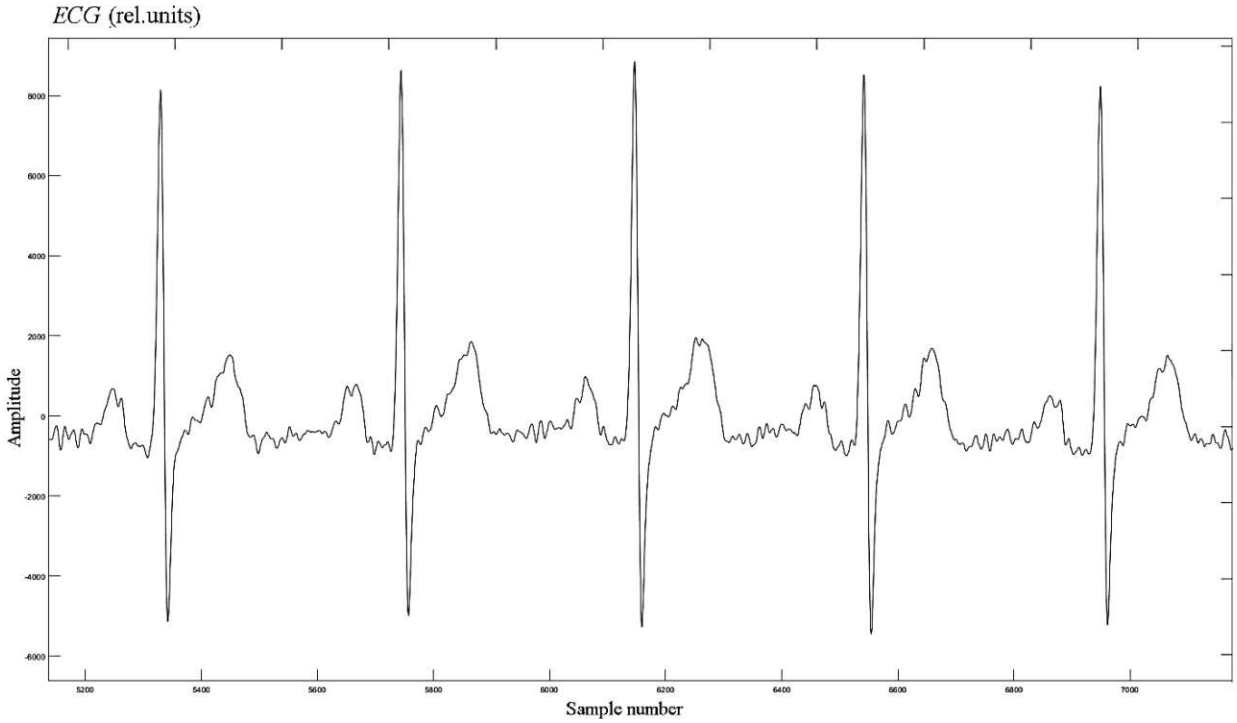

Figure 3.2.4 – Ten seconds windows of an ECG recording with MAX30001 using the best combination of the digital filters and gain.

During the initialization phase the FIFO length was set to 10. This means, that MATLAB should also read 10 samples. Every iteration, MATLAB is adding the last 10 samples at the end of an array, used to store the entire data recorded.

Figure 3.2.5 shows the beginning of a real time plot of the data. Since the recording just started, the 10 seconds window is not yet full. In Figures 3.2.5 through 3.2.7 how the 10 seconds window behaves at the start of a recording. A full 10 seconds window is presented in Figure 3.2.8.

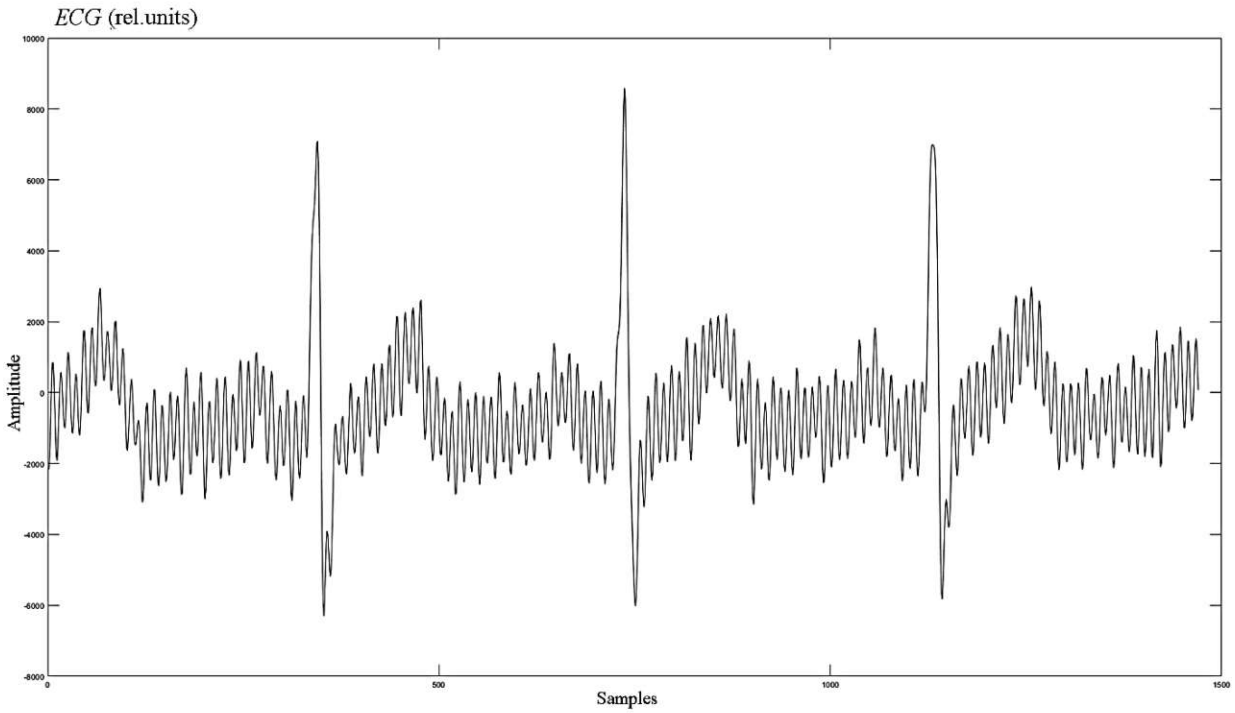

Figure 3.2.5 – Beginning of the real time plot. Only three R-peaks can be seen and a total of approximately 1500 samples

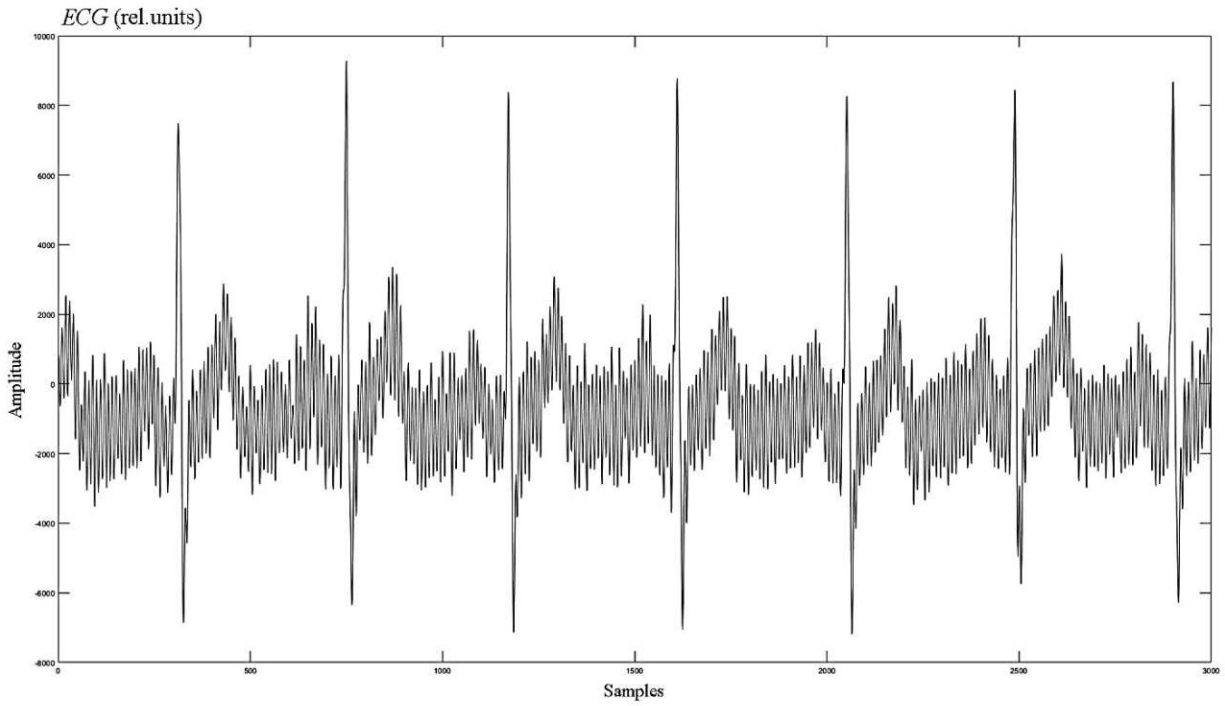

Figure 3.2.6 – Beginning of the real time plot. More R-peaks can be seen and a total of approximately 3000 samples

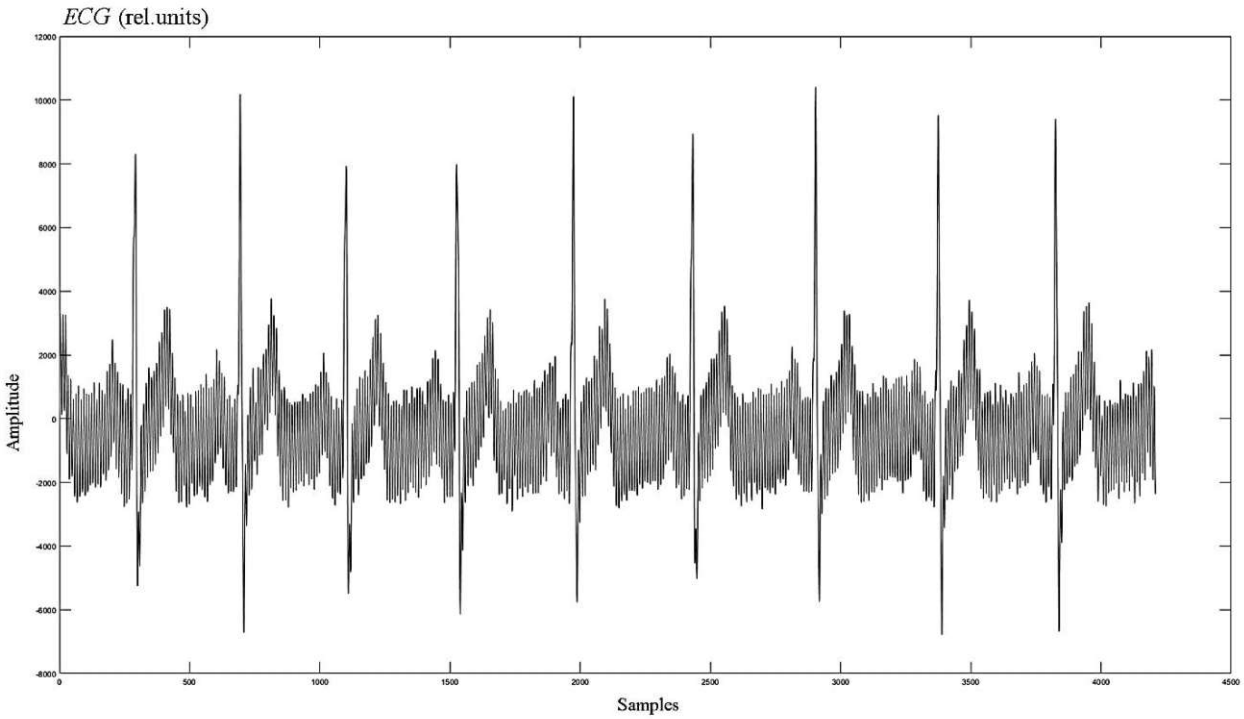

Figure 3.2.7 – Beginning of the real time plot. Even more R-peaks can be seen and a total of approximately 4300 samples

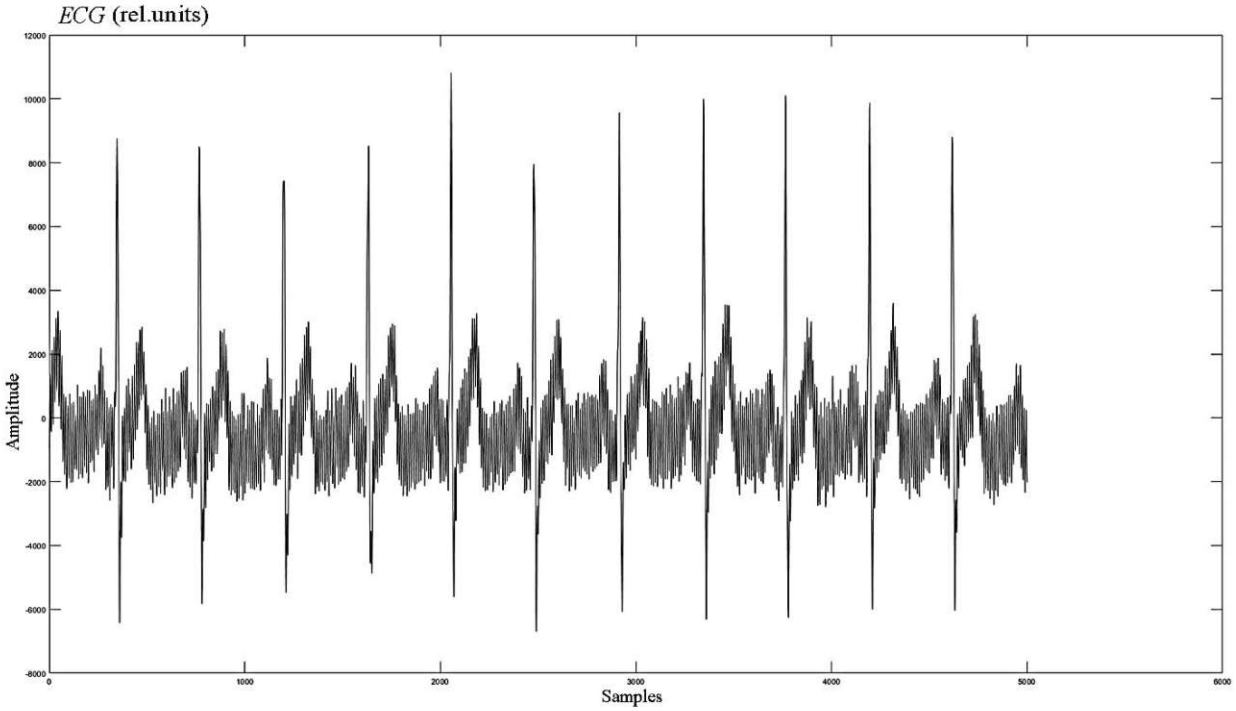

Figure 3.2.8 – Real time plot continuous ten seconds window. 5000 samples are constantly plotted to creating a moving window.

3.3 ADAPTIVE STIMULATION PLATFORM INTEGRATION

A platform for adaptive stimulation was previously developed in Simulink (Figure 3.3.1). This model used the BIOPAC system as the source of the biosignals. In order to simulate the entire model with the new system developed with MAX30001 at its core, some changes had to be made (Figure 3.3.2).

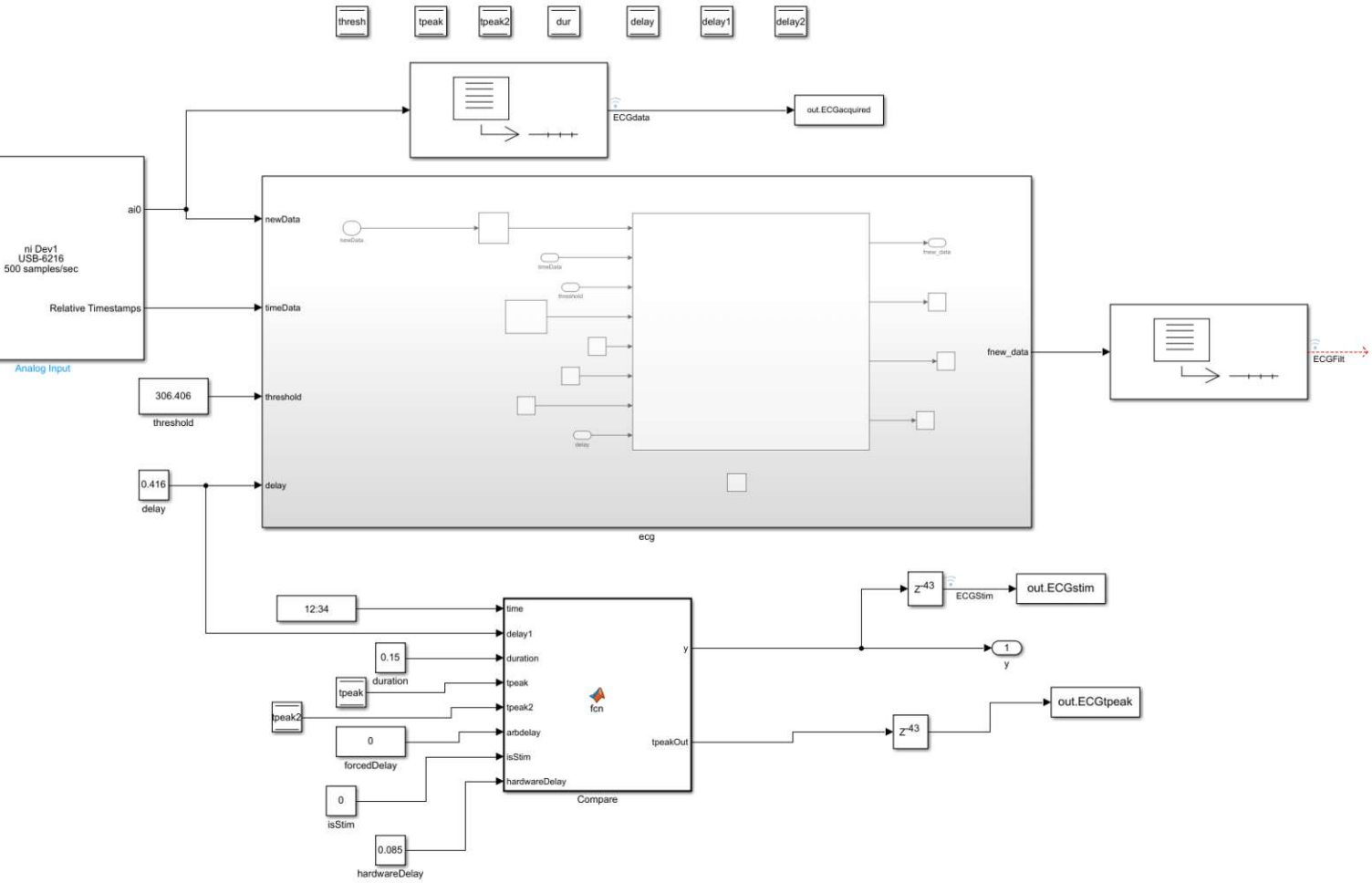

Figure 3.3.1 – Original Simulink model for the Adaptive stimulation platform

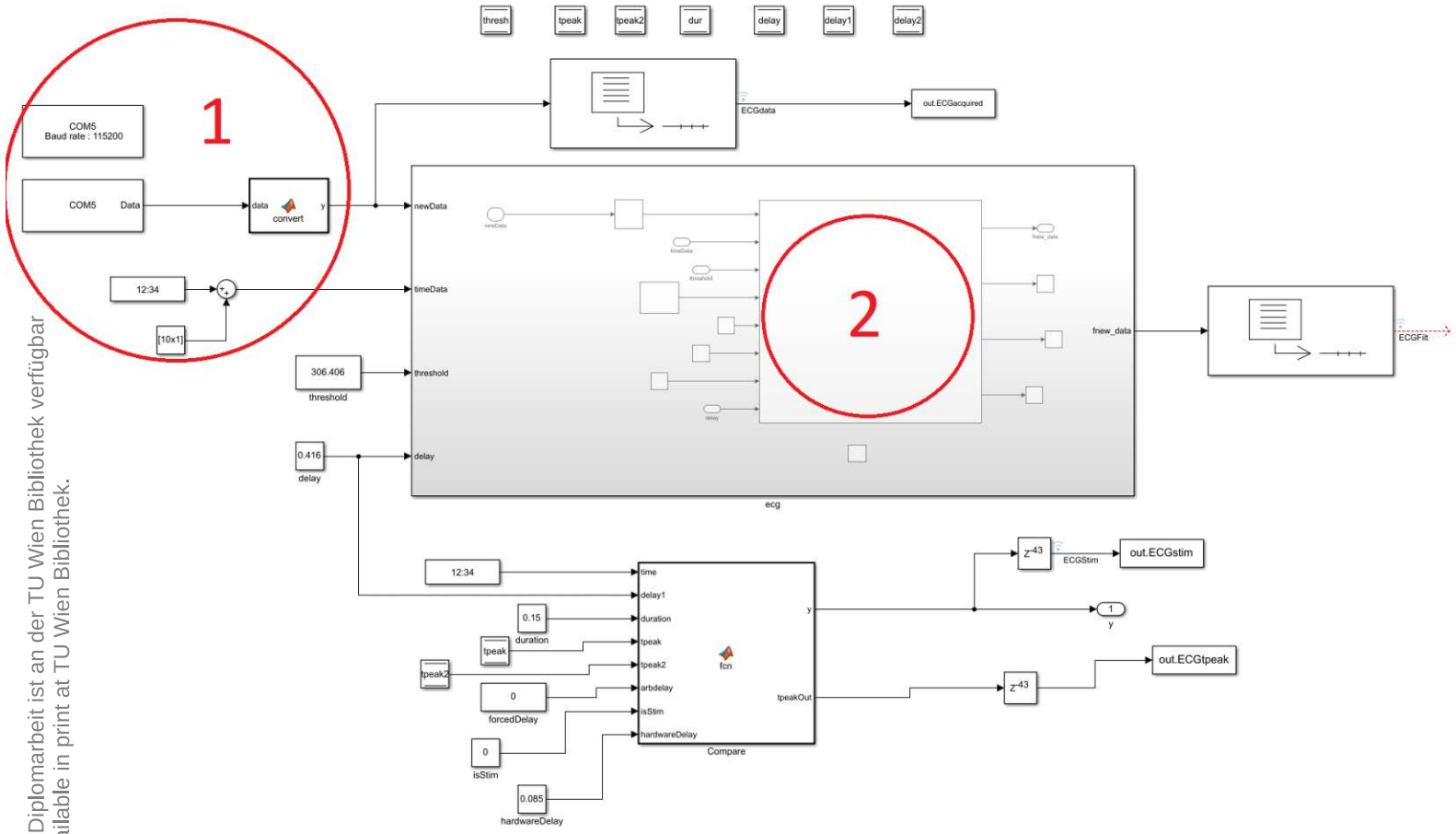

Figure 3.3.2 – Modified Simulink model for the Adaptive stimulation platform.

First and most important, the source of the data needed to be changed to the serial port to which the microcontroller was connected. The serial communication had to be configured using the same settings as before. Figurexx shows a few more settings for the serial block: data type (uint32), the header in hexadecimal format and the number of samples to be read after the header was identified. After the data was read, it had to be converted in signed magnitude; this was done running a MATLAB code within the simulation. At the same time, a timestamp generator had to be added, since the model needed an internally governed timestamp format.

Since MAX30001 has integrated filters, the post processing of the signal within the model is obsolete, therefore filters were removed from the model. Also, a hardware delay had to be taken into account, in order to compensate.

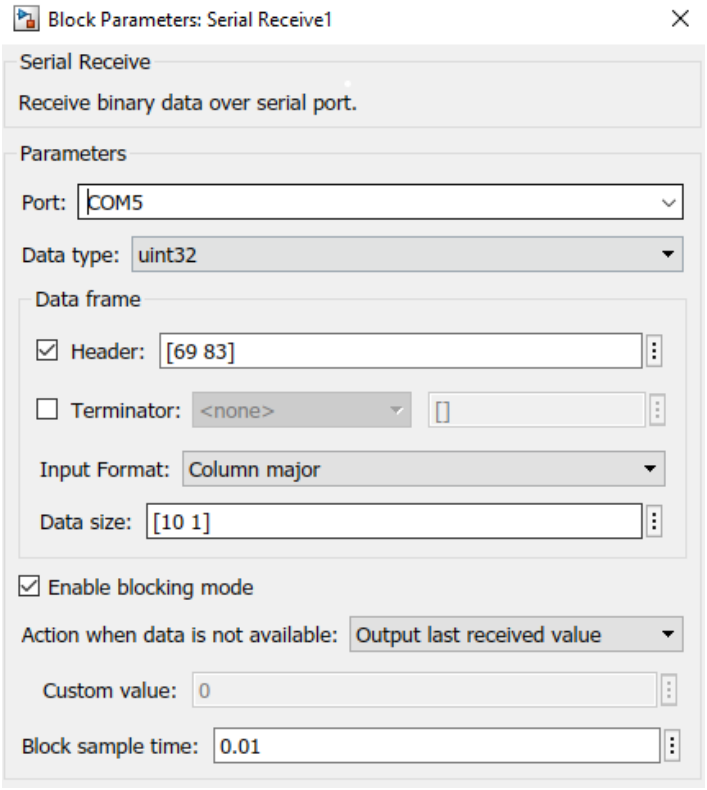

Figure 3.3.3 – Simulink serial port configuration

To run the simulation a calibration phase is needed. The model would compare a 20 seconds recording with an ECG waveform template. In order to achieve this calibration, a new ECG waveform template has been made. The template consists of a PQRST complex, that was extracted, averaged, and resampled, from approximately 180 seconds recording. While recording for the new template, some small movement artifacts also occurred. Creating the template with these artifacts, will allow the model to properly calibrate and work in real conditions. Figure 3.3.4 presents the approximately 3 minutes recording, from which, each PQRST complex was extracted. The extracted and overlapped PQRST complexes are shown in Figure 3.3.5. After this extraction, each complex was resampled, and then averaged, in order to arrive at the final template; shown in Figure 3.3.6.

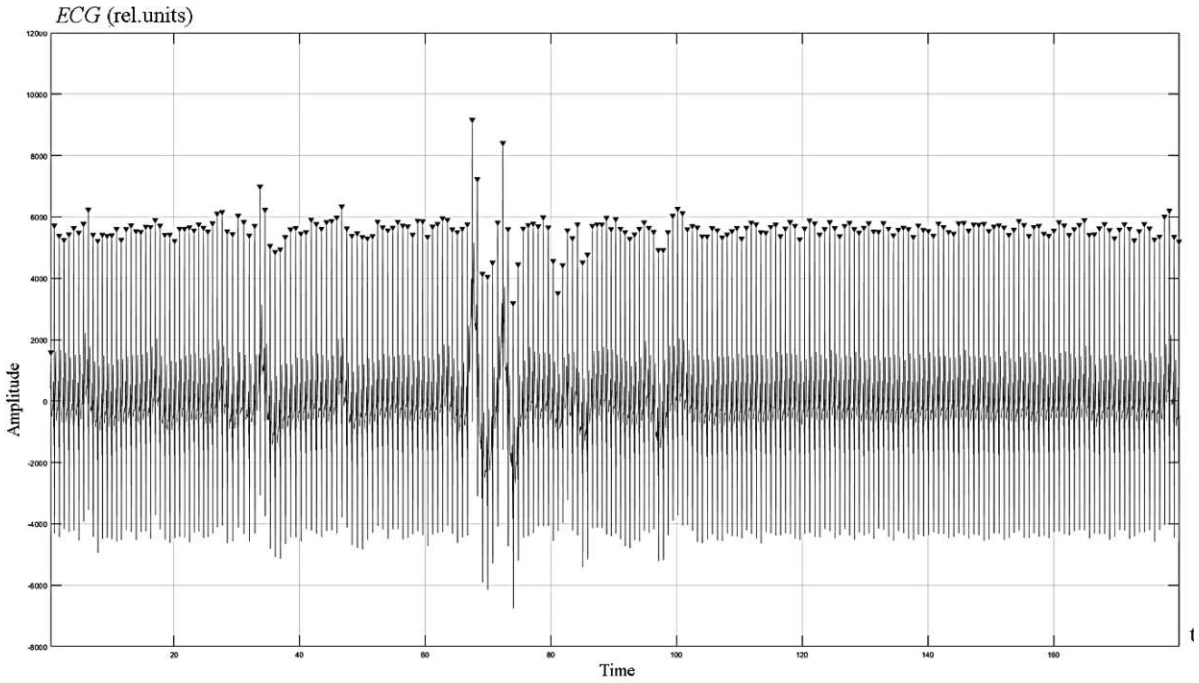

Figure 3.3.4 – Three minutes ECG recording. The R-peaks are identified, and some movement artifacts can be observed.

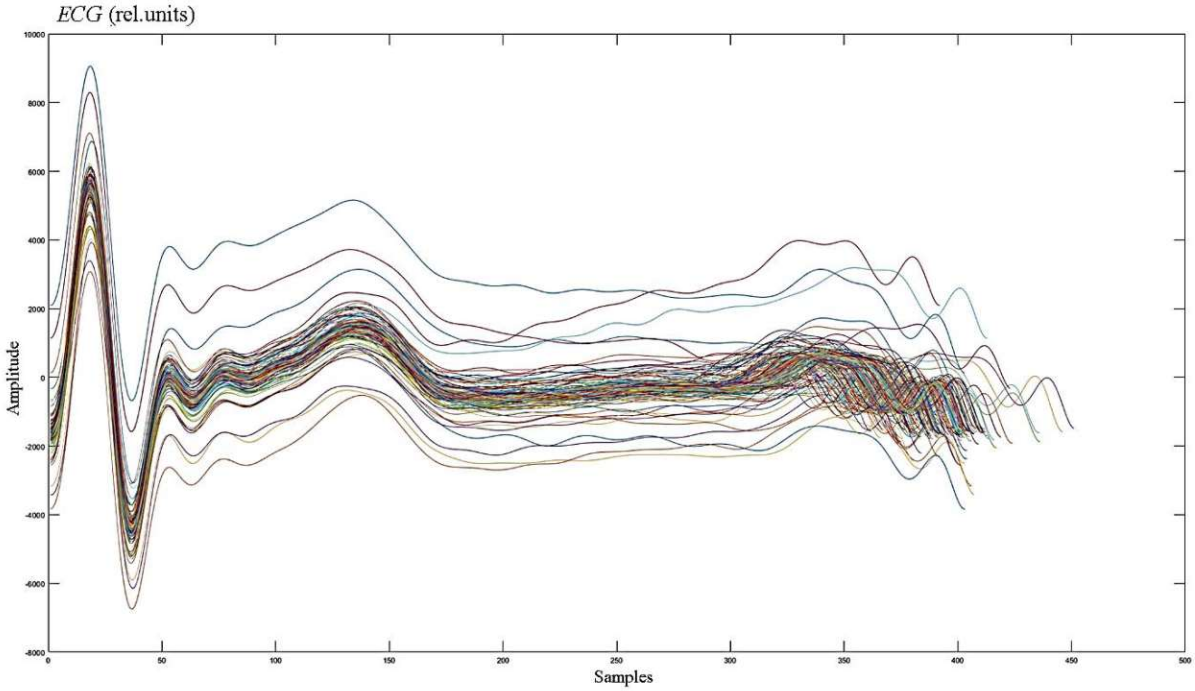

Figure 3.3.5 – The extracted QRSTP complexes from the 3 minutes recordin

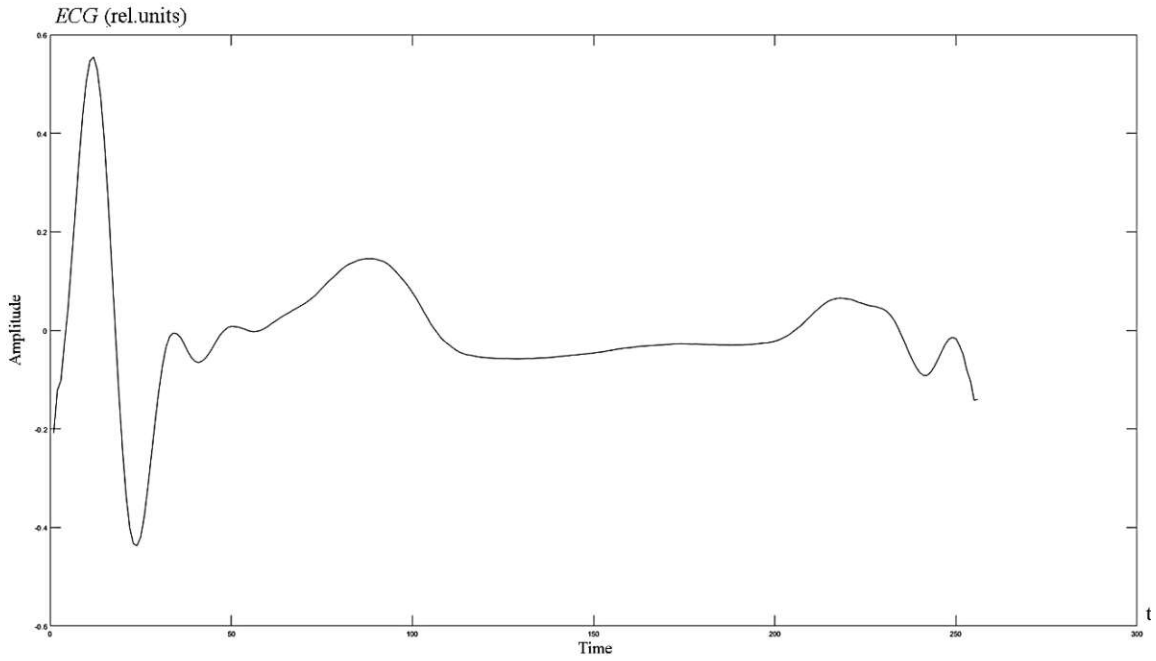

Figure 3.3.6 – ECG calibration template. The extracted QRSTP extracted complexes were averaged and resampled to create this template.

Figure 3.3.7 compares a failed calibration (A) with a successful one (B). The calibration error can be clearly seen, though the source of this error was most of the time the ECG waveform template. The template was imbued with some movement artifacts, to both replicate the behaviour in a real situation and to properly calibrate with the stimulator model.

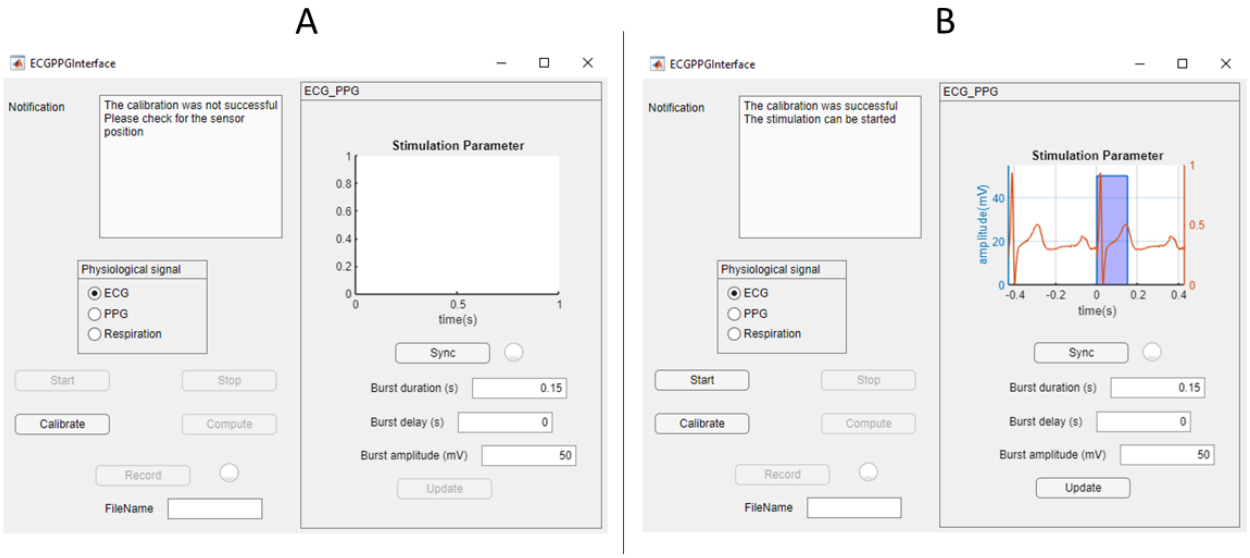

Figure 3.3.7 – Adaptive stimulation platform GUI. A – uncalibrated run; B – calibrated run.

Once calibrated, the simulation of the closed-loop biofeedback stimulation can start. For this a stimulation command was sent from the Simulink model, back to the microcontroller, where it was timestamped.

In Figure 3.3.8 and Figure 3.3.9 the stimulation signal starts close to the Q-peak and stops at the T-wave. The amplitude of the stimulation signal is constant at 50 mV and the burst duration is also constant at 0.15 seconds. These values were pre-set in the GUI of the adaptive stimulation platform and can be changed for each patient.

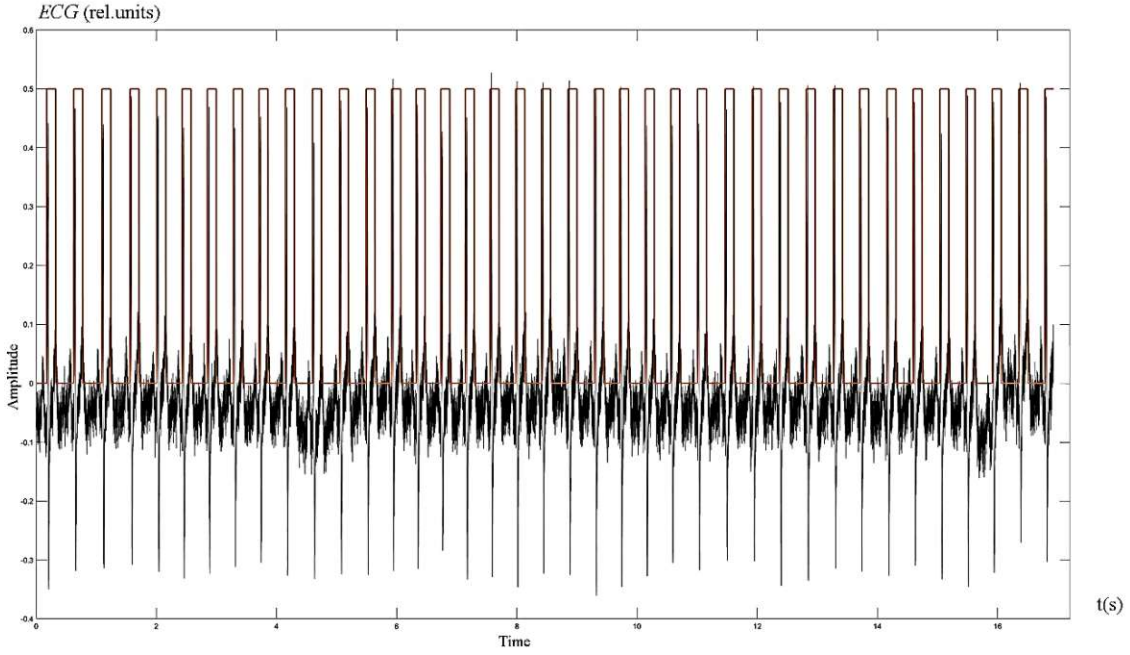

Figure 3.3.8 – A 17 seconds snippet from the simulation of the stimulation using the new system for the biofeedback.

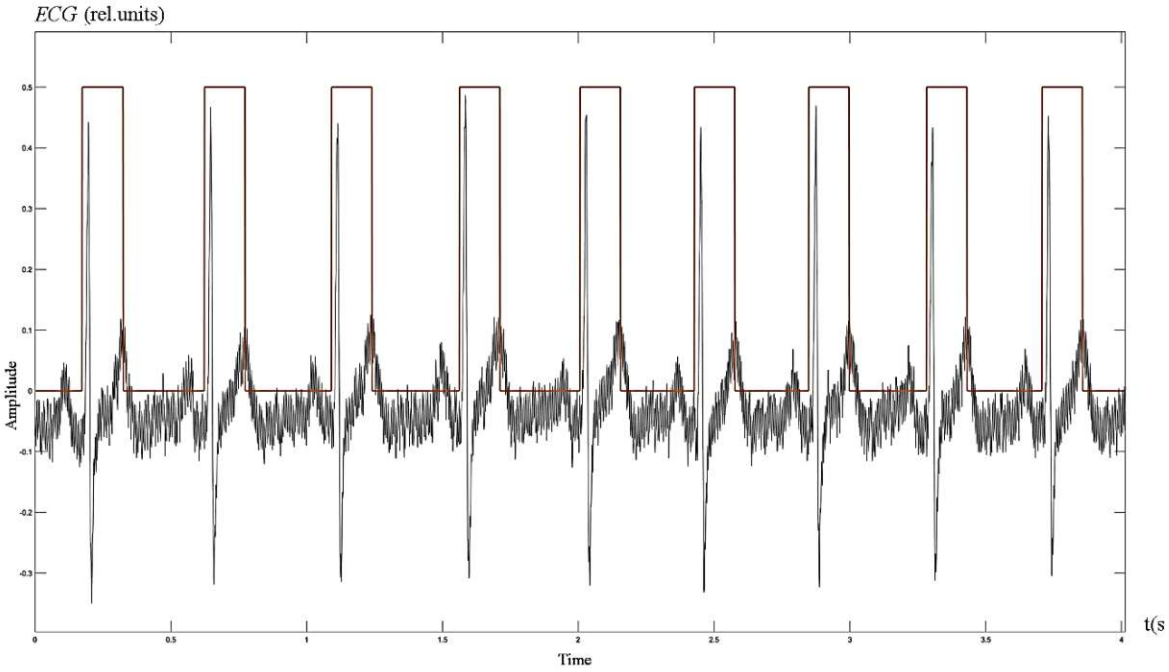

Figure 3.3.9 - Close up of the stimulation simulation.

3.4 COMPARING MAX30001 WITH BIOPAC

MAX30001 is a clinical grade ECG AFE. To confirm this and have a number for the overall latency of the system, a comparison was done with an already homologated device, BIOPAC MP36. Figure 3.4.1 shows the setup for this comparison.

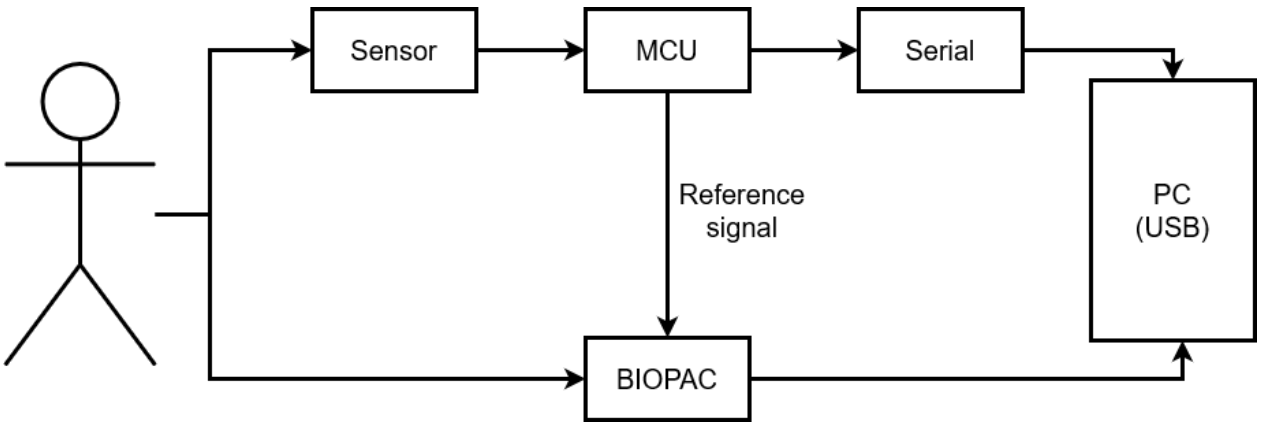

Figure 3.4.1 – Set up for comparing MAX30001 with MP36 device from BIOPAC

Each system has its own software for data acquisition, therefore a reference between the two devices was needed. For this, the microcontroller was programmed to send a reference analog signal to one of the channels of the BIOPAC system. This signal would mark the beginning of a recording on the microcontroller.

Four sets of recordings were made. Each set was recorded with a different method of storing the data from MAX30001. One set contains ten recordings with the MAX30001 and ten recordings with the MP36. The data from both devices was then imported in MATLAB and aligned for comparison. Figure 3.4.2 shows the ECG signals recorded with MAX30001 and MP36, as well as the reference signal. The signal form MAX30001 is not as smooth as the one from MP36, but the waveform is the same. The smoothness of the signal can be improved depending on the configuration and the electromagnetic noise around.

Aligning the two signals as seen in Figure 6.15, the reference signal can be used to calculate the latency of the MAX30001 compared to the MP36 system. Since the latency calculated here (3.4.1) is in comparison to another device, it is not an absolute value, it is only a theoretical one; the real latency might be different than the values obtained.

$$Latency_{\mathrm{MAX-BIOPAC}} = 84\,(82 \pm 2) \qquad ms \tag{3.4.1}$$

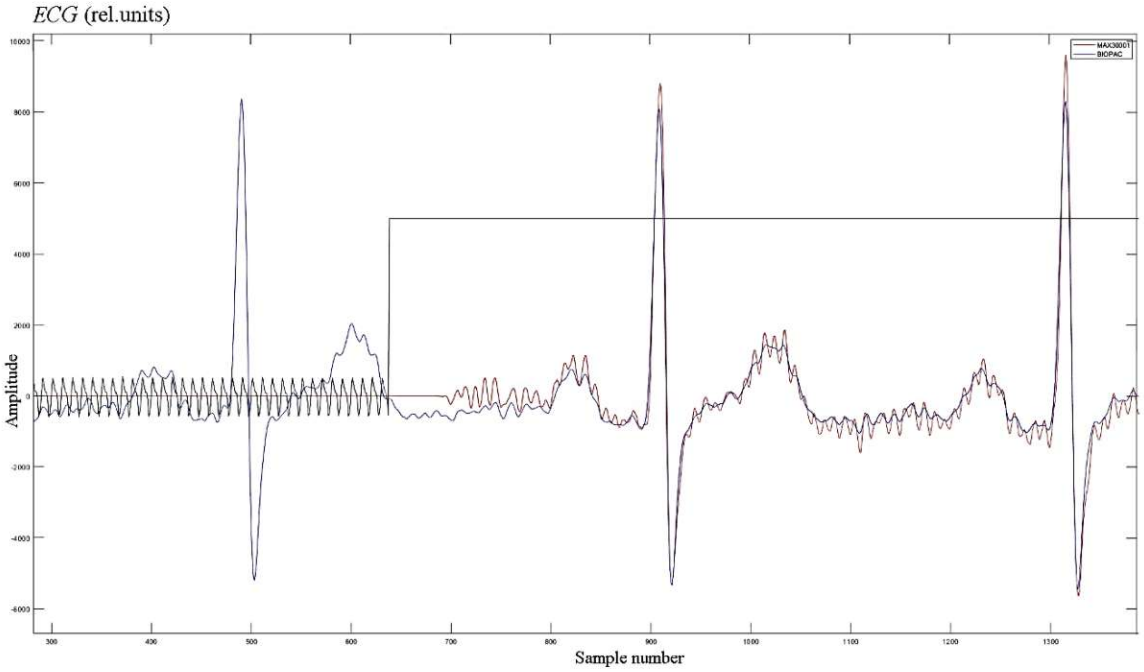

Figure 3.4.2 – ECG recordings from BIOPAC – blue; and MAX30001 – red. The Black signal is a reference signal sent fron the microcontroller to the BIOPAC at the start of the recording

To get a deeper understanding of the total theoretical latency of this work, a few more measurements were made. First, the amount of time it takes to read the ten samples from the sensor was measured. This latency was measured while only recording ECG and sending it to the PC. Equation (3.4.2) shows the result of this measurement. Going further and calculating the UART transmission baud rate and calculating for the ten samples that were sent, the result is approximately four milliseconds. Taking all of this into account, the latency of one iteration of reading and transmitting data adds up to approximately 24 milliseconds.

$$Latency_{\mathrm{ECG-UART}} = 22\,(\,20 \pm 2\,) \qquad ms \tag{3.4.2}$$

$$Latency_{\mathrm{UART}} = 6\,(\,4 \pm 2\,) \qquad ms \tag{3.4.3}$$

4 DISCUSSION AND FUTURE WORK

The aim of this thesis was to validate the use of the MAX30001 sensor for biofeedback in a closed-loop auricular vagus nerve stimulation device. The current stimulator used the BIOPAC MP36 system, which required a personal computer to operate. By incorporating an integrated circuit that can record biosignals, the stimulator could become completely independent, which could lead to a wearable device that is easy for patients to use in their daily lives.

To ensure that MAX30001 is the best option for this application, it was compared to four other biosensors based on their datasheet and specifications, as well as the type of biosignals they record. A study by Elena Schrödl et al (2019) found that while pulse rate variability (PRV) derived from photoplethysmography (PPG) is a suitable biosensor for this application, it is susceptible to movement artifacts, which can result in an overestimation of ten milliseconds in the PPG signal compared to the electrocardiogram (ECG) signal. Given these results and considering the influence of respiration on the vagus nerve (Sclocco, 2019), as well as the variety of integrated circuits available, it is reasonable to choose a sensor that provides both ECG and bioimpedance to measure respiration. MAX30001 was identified as the best option for this application since it was the only one able to record both biosignals.

The STM LQFP64 microcontroller was used to control the MAX30001 sensor since the stimulator was already developed with it. The sensor uses the SPI protocol at speeds up to 12 MHz to communicate with the microcontroller. A new library was defined to use the sensor, within which all usable registers of MAX30001 were defined, as well as communication, configuration, reading, and data saving functions. Initially a serial monitor was used to verify the inner workings of the sensor. After that, a program was developed in MATLAB for data recording, analysis, and real-time visualization.

One limitation of the study is the difficulty in recording both electrocardiogram (ECG) and bioimpedance (BioZ) simultaneously using the MAX30001 sensor. During initial trials, a pseudo-simultaneous recording method was attempted by using a timer to switch between the active module. However, this resulted in data loss and difficulty in reading the recorded data. Further research is needed to investigate methods for achieving simultaneous or near-simultaneous recording of ECG and BioZ with minimal data loss.

The new biofeedback system was then compared to the BIOPAC MP36 system, and it was found that the new system was able to acquire data with comparable accuracy. The new system was also

integrated with a simulation platform for adaptive auricular vagus nerve stimulation, and it was found that the system worked seamlessly with the stimulator.

While these results are positive, there is still work to be done before the MAX30001 sensor can be used at its full potential in a closed-loop biofeedback auricular vagus nerve stimulation device. One important step would be to validate the BioZ module of the sensor. Additionally, the sensor would need to be integrated into a custom PCB, which would also contain the microcontroller and stimulator, so that a firmware can be developed that includes both data acquisition and stimulation.

Further testing and validation would be required to ensure the safety and efficacy of the device when used in a clinical setting. This would involve conducting clinical trials and gathering data on the device's performance and any potential side effects. It is also important to consider factors such as ease of use and patient comfort in the design of the device. With these considerations in mind, the device has the potential to be a valuable tool in the treatment of various conditions that can be treated through vagus nerve stimulation.

5 REFERENCES

Badran B. W., Mithoefer, O. J., Summer, C. E., LaBate, N. T., Glusman, C. E., Badran, A. W., et al. Short trains of transcutaneous auricular vagus nerve stimulation (taVNS) have parameter-specific effects on heart rate [Journal]. - [s.l.] : Brain Stimulation, 2018b. - Vol. 11. - pp. 699-708.

Bermejo P., Lopez, M., Larraya, I., Chamorro, J., Cobo, J. L., Ordonez, S., et al. Innervation of the human cavum conchae and auditory canal: [Journal]. - [s.l.] : BioMed Research International, 2017. - Vol. 2017.

Berthoud H. R., and Neuhuber, W. L. Functional and chemical anatomy [Journal]. - [s.l.] : Autonomic Neuroscience, 2000.

Boon K. H., Khalil-Hani, M., Malarvili, M. B., and Sia, C. W. Paroxysmal atrial fibrillation prediction method with shorter HRV sequences [Journal]. - [s.l.] : Computer Methods and Programs in Biomedicine, 2016. - Vol. 134. - pp. 187-196.

Boon P., Vonck, K., van Rijckevorsel, K., Tahry, E. R., Elger, C. E., Mullatti, N., et al. A prospective, multicenter study of cardiac-based seizure detection to activate vagus nerve stimulation [Journal]. - [s.l.] : Seizure, 2015. - Vol. 32. - pp. 52-61.

Brown G. L., and Eccles, J. C. The action of a single vagal volley on the rhythm of the heart beat [Journal]. - [s.l.] : Journal of Physiology, 1934. - 2 : Vol. 82. - pp. 211-241.

Duncan A. Groves Verity J. Brown Vagal nerve stimulation: a review of its applications and potential mechanisms that mediate its clinical effects [Journal]. - [s.l.] : Neuroscience & Biobehavioral Reviews, 2005. - 3 : Vol. 29.

Elena Schrödl Stefan Kampusch, Babak Dabiri Razlighi, Van Hoang Le, Jozsef Constantin Széles, Eugenijus Kaniusas Feasibility of pulse rate variability as feedback in closed-loop percutaneous auricular vagus nerve stimulation [Journal]. - [s.l.] : Vibroengineering PROCEDIA, 2019. - Vol. 26. - pp. 35-39.

Elliott RE Morsi A, Kalhorn SP, et al. Vagus nerve stimulation in 436 consecutive patients with treatment-resistant epilepsy: long-term outcomes and predictors of response. [Journal]. - [s.l.] : Epilepsy & Behavior, 2011. - 1 : Vol. 20. - pp. 57-63.

Foley J.O., and DuBois, F.S. Quatitative studies of the vagus nerve in the cat. I. The ratio of sensory to motor fibers. I. The ratio of sensory to motor fibers [Journal] // J. Comp. Neurol.. - [s.l.] : J. Comp. Neurol. 67, 49-67, 1937. - pp. 49-67.

Frei M. G., and Osorio, I. Left vagus nerve stimulation with the neurocybernetic prosthesis has complex effects on heart rate and on its variability in humans. [Journal]. - [s.l.] : Epilepsia, 2001. - 8 : Vol. 42.

Gao X.-Y., Zhang, S.-P., Zhu, B., and Zhang, H.-Q. Investigation of specificity of auricular acupuncture points in regulation of autonomic function in anesthetized rats [Journal]. - [s.l.] : Autonomic Neuroscience, 2007. - 1-2 : Vol. 138. - pp. 50-56.

Gaul C., Diener, H. C., Silver, N., Magis, D., Reuter, U., Andersson, A., et al. Non-invasive vagus nerve stimulation for PREVention and Acute treatment of chronic cluster headache (PREVA): a randomised controlled study [Journal]. - [s.l.] : Cephalalgia, 2016. - 6 : Vol. 36. - pp. 534-546.

Grant P. F., and Lowery, M. M. Simulation of cortico-basal ganglia oscillations and their suppression by closed loop deep brain stimulation [Journal]. - [s.l.] : IEEE Transactions on Neural Systems and Rehabilitation Engineering, 2012. - 4 : Vol. 21. - pp. 584-594.

Gray Henry. Henry Vandyke Carter Anatomy of the Human Body [Book]. - [s.l.] : Lea & Febiger, 198. - 20.

Groves D. A., and Brown, V. J. Vagal nerve stimulation: a review of its applications and potential mechanisms that mediate its clinical effects [Journal]. - [s.l.] : Neuroscience & Biobehaviour, May 2005. - 3 : Vol. 29. - pp. 493-500.

He W., Zhu, B., Zhu, X.-L., Li, L., Bai, W.-Z., and Ben, H. The auriculo-vagal afferent pathway and its role in seizure suppression in rats [Journal]. - [s.l.] : BMC Neuroscience, 2013. - 85 : Vol. 14.

Johnson RL Wilson CG A review of vagus nerve stimulation as a therapeutic intervention [Journal]. - [s.l.] : Journal of Inflammation Research, 2018. - Vol. 11.

Kampusch S., Kaniusas, E., Thürk, F., Felten, D., Hofmann, I., and Szeles, C. Device development guided by user satisfaction survey on auricular vagus nerve stimulation [Journal]. - [s.l.] : Current Directions in Biomedical Engineering, 2016. - 1 : Vol. 2. - pp. 593-597.

Kaniusas E., Kampusch, S., Tittgemeyer, M., et al. Current directions in the auricular vagus nerve stimulation I - A physiological perspective [Journal]. - [s.l.] : Frontiers in Neuroscience, 2019.

Kaniusas E., Kampusch, S., Tittgemeyer, M., Panetsos, F., Gines, R.F., Papa, M., Kiss, A., Podesser, B., Cassara, A.M., Tanghe, E., Samoudi, A.M., Tarnaud, T., Joseph, W., Marozas, V., Lukosevicius, A., Ištuk, N., Lechner, S., Klonowski, W. Current Directions in the Auricular Vagus Nerve Stimulation II – An Engineering Perspective [Journal]. - [s.l.] : Frontiers in Neuroscience, 2019. - Vol. 13.

Liporace J., Hucko, D., Morrow, R., Barolat, G., Nei, M., Schnur, J., et al. Vagal nerve stimulation: adjustments to reduce painful side effects [Journal]. - [s.l.] : Neurology, 2001. - Vol. 57. - pp. 885-886.

MaximIntegrated MAX30001 Ultra-Low-Power, Single-Channel Integrated Biopotential (ECG, R-to-R, and Pace Detection) and Bioimpedance (BioZ) AFE. - 08 2019. - 19-100133.

Mertens A., Raedt, R., Gadeyne, S., Carrette, E., Boon, P., and Vonck, K. Recent advances in devices for vagus nerve stimulation. [Journal]. - [s.l.] : Expert Review of Medical Devices, 2018. - 8 : Vol. 15.

Monkhouse Stanley Cranial Nerves. Functional Anatomy [Book]. - [s.l.] : Cambridge University Press, 2005.

Nomura S., and Mizuno, N. Central distribution of primary afferent fibers in the Arnold's nerve (the auricular branch of the vagus nerve): a transganglionic HRP study in the cat. [Journal]. - [s.l.] : Brain Research, 1984. - 2 : Vol. 292. - pp. 199-205.

Onuora S. Vagus nerve stimulation reduces RA severity in patients. [Journal]. - [s.l.] : Nat Rev Rheumatol, 2016. - 9 : Vol. 12.

Peuker E.T., and Filler, T.J. The Nerve supply of the human auricle [Journal]. - [s.l.] : Clinical Anatomy, 2002. - Vol. 15. - pp. 35-37.

Polyvagal theory for Dummies [Online] // Movement meets life. - 10 10 2022. - https://www.movementmeetslife.com/en/posts/polyvagal-theory-for-dummies.

Roberts A., Sithole, A., Sedghi, M., Walker, C. A., and Quinn, T. M. Minimal adverse effects profile following implantation of periauricular percutaneous electrical nerve field stimulators: a retrospective cohort study [Journal]. - [s.l.] : Medical Devices : Evidence and Research, 2016. - Vol. 2016:9. - pp. 389-393.

S. Kampusch E. Kaniusas and J. C. Széles New approaches in multi-punctual percutaneous stimulation of the auricular vagus nerve [Conference] // 6th International IEEE/EMBS Conference on Neural Engineering (NER). - 2013. - pp. 263-266.

Safi J. The organization and function of endogenous antinociceptive systems [Journal]. - [s.l.] : Progress in Neurobiology, 1996. - Vol. 50. - pp. 49-81.

Salam M. T., Velazquez, J. L. P., and Genov, R. Seizure suppression efficacy of closed-loop versus open-loop deep brain stimulation in a rodent model of Epilepsy [Journal]. - [s.l.] : IEEE Transactions on Neural Systems and Rehabilitation Engineering, 2015. - 6 : Vol. 24. - pp. 710-719.

Sclocco R., Garcia, R. G., Kettner, N. W., Isenburg, K., Fisher, H. P., Hubbard, C. S., et al. The influence of respiration on brainstem and cardiovagal response to auricular vagus nerve stimulation: A multimodal ultrahigh-field (7T) fMRI study [Journal]. - [s.l.] : Brain Stimulation, 2019. - Vol. 12. - pp. 911-921.

Spuck S Tronnier V, Orosz I, Schönweiler R, Sepehrnia A, Nowak G, Sperner J. Operative and technical complications of vagus nerve stimulator implantation. [Journal]. - [s.l.] : Neurosurgery, 2010. - 489-94 : Vol. 67(2 Suppl Operative).

Standring S. Gray's Anatomy, the Anatomical Basis of Clinical Practice [Book]. - [s.l.] : Edn. Amsterdam: Elsevier, 2016. - 41st.

Stanslaski S., Afshar, P., Cong, P., Giftakis, J., Stypulkowski, P., Carlson, D.,et al. Design and validation of a fully implantable, chronic, closed-loop neuromodulation device with concurrent sensing and stimulation [Journal]. - [s.l.] : IEEE Transactions on Neural Systems and Rehabilitation Engineering, July 2012. - 4 : Vol. 20. - pp. 410-421.

STMicroelectronics STM32CubeMX for STM32 configuration and initialization C code generation. - [s.l.] : STMicroelectronics, June 2022. - Vol. UM1718 Rev 38.

Straube A., Ellrich, J., Eren, O., Blum, B., and Ruscheweyh, R. Treatment of chronic migraine with transcutaneous stimulation of the auricular branch of the vagal nerve (auricular t-VNS): a randomized, monocentric clinical trial. [Journal]. - [s.l.] : Journal of Headache and Pain, 2015. - 63 : Vol. 16. - pp. 1-9.

Thayer Julian F. , Shelby S. Yamamoto, Jos F. Brosschot The relationship of autonomic imbalance, heart rate variability and cardiovarsular disease risk factors [Journal]. - [s.l.] : International Journal of Cadiology, 2009.

Thompson N., Ravagli, E., Mastitsakaya, S., Iacoviello, F., Aristovich, K., Perkins, J., et. al. MicroCT optimisation for imaging fascicular anatomy in [Journal] // J. Neurosci.. - 2020.

Trepel Martin Neuroanamy - Structure and function [Buch]. - München : Elsevier, 2017.

Val-Laillet D Biraben A, Randuineau G, Malbert CH. Chronic vagus nerve stimulation decreased weight gain, food consumption and sweet craving in adult obese minipigs. [Journal]. - [s.l.] : Appetite, 2010. - 2 : Vol. 55. - pp. 245-252.

6 TABLE OF FIGURES

Figure 1.1.1 – Vagus nerve pathway (Polyvagal theory, 2022) 7

Figure 1.1.2 - Plan of upper portions of glossopharyngeal, vagus, and accessory nerves. (Gray, 1918) 8

Figure 1.3.1 – Invasive, cervical vagus nerve stimulator. (Onuora, 2016) 12

Figure 1.3.2 – aVNS electrode placement. Inspired from (Kaniusas, 2019) 13

Figure 1.4.1 – Open loop Vagus nerve stimulation flow 14

Figure 1.4.2 – Closed loop vagus nerve stimulation flow 15

Figure 2.1.1 – AD8232 schematic. 18

Figure 2.1.2 – Texas Instrumens AFE 4900 schematic 19

Figure 2.1.3 – MaximIntegrated MAX86150 schematic 19

Figure 2.1.4 - MaximIntegrated MAX30001 schematic 21

Figure 2.2.1 – STM LQFP64 microcontroller chip pinout. 22

Figure 2.2.2 – STM32 Nucleo-G431RE development board pinout. 23

Figure 2.2.3 – STM CubeMX software. Show the pin configuration of the microcontroller 24

Figure 2.5.1 – RealTerm serial monitor software. 26

Figure 2.6.1 – BIOPAC MP36R device. 27

Figure 2.7.1 – MAX30001EVSYS – evaluation kit for MAX30001. Focus on the MAX30001 chipset. 28

Figure 2.7.2 – MAX30001 evaluation kit GUI. In the figure the settings for the ECG channel can be seen.. 28

Figure 2.7.3 – MAX30001 evaluation kit GUI. This figure shows the ECG MUX settings. 29

Figure 2.7.4 – Electrode placement for ECG recording. A – chest placement; B – Arms and right leg placement. Blue – negative electrode; Red – positive electrode; Black – body bias drive. 29

Figure 2.7.5 – MAX30001 electrical schematic with power supply elements. 30

Figure 2.7.6 – MAX30001 internal FIFO structure. 32

Figure 3.1.1 – High level flow diagram of the program. 33

Figure 3.1.2 – MAX30001 configuration function flow diagram. 34

Figure 3.1.3 – Interrupts function flow diagram. 37

Figure 3.1.4 – Main loop flow diagram 38

Figure 3.1.5 – ECG read function flow diagram. 39

Figure 3.1.6 – LQFP64 clock tree diagram with focus on the Real Time clock (RTC) sources and configuration 40

Figure 3.1.7 - The flow of sending data from the microcontroller 42

Figure 3.1.8 – Internal structure of the Flash memory of LQFP64 43

Figure 3.2.1 – MATLAB program flow diagram 44

Figure 3.2.2 – Ten seconds windows of an ECG recording with MAX30001 without using the digital filters 45

Figure.3.2.3 – Ten seconds windows of an ECG recording with MAX30001 with digital filters activated. 46

Figure 3.2.4 – Ten seconds windows of an ECG recording with MAX30001 using the best combination of the digital filters and gain. 46

Figure 3.2.5 – Beginning of the real time plot. Only three R-peaks can be seen and a total of approximately 1500 samples 47

Figure 3.2.6 – Beginning of the real time plot. More R-peaks can be seen and a total of approximately 3000 samples 48

Figure 3.2.7 – Beginning of the real time plot. Even more R-peaks can be seen and a total of approximately 4300 samples 48

Figure 3.2.8 – Real time plot continuous ten seconds window. 5000 samples are constantly plotted to creating a moving window. 49

Figure 3.3.1 – Original Simulink model for the Adaptive stimulation platform 50

Figure 3.3.2 – Modified Simulink model for the Adaptive stimulation platform. 51

Figure 3.3.3 – Simulink serial port configuration 52

Figure 3.3.4 – Three minutes ECG recording. The R-peaks are identified, and some movement artifacts can be observed. 53

Figure 3.3.5 – The extracted QRSTP complexes from the 3 minutes recordin 53

Figure 3.3.6 – ECG calibration template. The extracted QRSTP extracted complexes were averaged and resampled to create this template. 54

Figure 3.3.7 – Adaptive stimulation platform GUI. A – uncalibrated run; B – calibrated run. 54

Figure 3.3.8 – A 17 seconds snippet from the simulation of the stimulation using the new system for the biofeedback. 55

Figure 3.3.9 - Close up of the stimulation simulation. 56

Figure 3.4.1 – Set up for comparing MAX30001 with MP36 device from BIOPAC 56

Figure 3.4.2 – ECG recordings from BIOPAC – blue; and MAX30001 – red. The Black signal is a reference signal sent fron the microcontroller to the BIOPAC at the start of the recording 58

7 TABLE OF TABLES

Table 2.1 – Materials used for this work 16
Table 2.1.1 – Sensor feature comparison 17
Table 2.7.1 – Pin configuration for SPI communication 31
Table 3.1.1 – Registers used to configure the ECG channel 34
Table 3.1.2 – All possible configurations for the ECG channel 35
Table 3.1.3 – Native Timestamp structures 40
Table 3.1.4 – UART communication protocol configuration 41